Available online at www.sciencedirect.com
SCIENCE DIRECT®
Computer Coupling of Phase Diagrams and Thermochemistry 28 (2004) 15–40
www.elsevier.com/locate/calphad

Progress in the thermodynamic modelling of the O–U–Zr ternary system

Pierre-Yves Chevalier*, Evelyne Fischer, Bertrand Cheynet

THERMODATA - INPG - CNRS, 6, rue du Tour de l'Eau, 38400 Saint-Martin-d'Hères, France

Received 5 January 2004; received in revised form 19 March 2004; accepted 19 March 2004
Available online 22 April 2004

Abstract

The thermodynamic modelling of the O–U–Zr system is part of the basic knowledge of the corium, mixture formed at high temperature between fuel and other materials of the vessel (zircalloy, steel, control rods, ...), which may interact with the concrete basemat during an hypothetical severe nuclear accident. Inconsistencies were previously detected in the available experimental information, phase diagram and thermodynamic properties, especially concerning the solubility of oxygen in uranium–zirconium liquid alloys and the extent of the oxygen–uranium liquid miscibility gap in the ternary system. The critical assessment was significantly improved in this work, both for the binary O–U, O–Zr, O_2U–O_2Zr, U–Zr, and the O–U–Zr ternary systems, taking into account the most recent experiments and evaluating ternary parameters for the main liquid and solid solutions. Calculated and experimental isothermal or isopleth phase diagrams are in satisfactory agreement, both qualitatively and quantitatively. However, experimental uncertainties still remain at high temperature.

Keywords: O–U–Zr; Thermodynamics; Modelling; Corium; Nuclear; Assessment

1. Introduction

The thermodynamic modelling of the O–U–Zr system is of first importance in the development of a reliable nuclear thermodynamic database for nuclear safety applications [1, 2]. This work was supported by the European Community through the CIT (corium interaction and thermochemistry) [3] and ENTHALPY (European nuclear thermodynamic database) [4] projects. In the unlikely event of a severe accident, all materials of a nuclear plant may interact thermochemically: fuel (UO_2), zircalloy (Zr), steel structures (Fe, Cr, Ni), control rods (Ag, Cd, In or B, C), selected fission products (Ba, La, Ru, Sr), concrete (Al_2O_3, CaO, FeO, Fe_2O_3, MgO, SiO_2), water and air (H, O). This inventory allows to identify the main components to be taken into account. Then, the thermodynamic modelling of the complex multicomponent system is based on the critical assessment of all the binary and the most important higher-order sub-systems (metallic, oxide, metal–oxide/oxygen), following the well known Calphad method.

As the first step of a severe accident, the fuel rods may melt and interact with other materials, leading to the core degradation. At high temperature, UO_2 reacts with the metallic zircalloy and is partially disintegrated. A ceramic solid solution $(U, Zr)O_{2\pm x}$ in equilibrium with a ternary (O–U–Zr) liquid phase is formed. The liquid presents a miscibility gap in the O–U system which extends into the ternary system. The thermochemical properties (liquidus, solidus, phase proportions, liquid miscibility gap) are needed to feed more global thermal hydraulic safety codes dedicated to the in-vessel core degradation, and must be validated by a very precise knowledge of the O–U–Zr ternary system.

Thus, the thermodynamic modelling of the O–U–Zr ternary system was undertaken by Chevalier and Fischer [5], from a critical assessment of all the available experimental information, on equilibrium phase diagram and thermodynamic properties. An optimisation procedure, developed by Lukas et al. [6], was used for the binary O–U, O–Zr, U–Zr and quasi-binary UO_2–ZrO_2 sub-systems. For the O–U–Zr ternary system, the ternary interaction parameters were adjusted by using some simple assumptions.

Unfortunately, at that time, the experimental information provided by different sources was not consistent in some specific fields. Moreover, new experimental results are now available, in particular in the binary (O–U), quasi-binary

* Corresponding author.
E-mail address: pierre-yves.chevalier@grenet.fr (P.-Y. Chevalier).
URL: http://thermodata.online.fr.

0364-5916/$ - see front matter © 2004 Elsevier Ltd. All rights reserved.
doi:10.1016/j.calphad.2004.03.005

(UO_2–ZrO_2) and ternary O–U–Zr systems, such as activity measurements in single-phase and two-phase regions, tie lines in liquid–solid and liquid–liquid fields, and liquidus and solidus temperatures.

It is why a new critical assessment of the O–U–Zr system was carried out in this work, consisting of the re-assessment of the O–U, O–Zr, O_2U–O_2Zr, U–Zr systems [6] and the optimisation of O–U–Zr interaction parameters, by using the Parrot software included in the Thermocalc computational tool [7]. The thermodynamic models used for solution phases and the assessment method are detailed in the following.

2. Thermodynamic modelling and assessment method

The thermodynamic models used for each solution phase will be detailed in the following.

The ternary liquid phase, L, was described with a non-ideal associate model between pure components, O_1(L), U_1(L), Zr_1(L), and associate species O_2U_1(L) and O_2Zr_1(L), with the formula: $(O_1, O_2U_1, O_2Zr_1, U_1, Zr_1)_1$. It generates eight binary and quasi-binary interaction parameters, $L(O_1, O_2U_1)$; $L(O_1, U_1)$; $L(O_2U_1, U_1)$; $L(O_1, O_2Zr_1)$; $L(O_1, Zr_1)$; $L(O_2Zr_1, Zr_1)$; $L(U_1, Zr_1)$; $L(O_2U_1, O_2Zr_1)$, and two ternary ones, $L(O_2U_1, Zr_1)$; $L(O_2Zr_1, U_1)$. O_1 allows to describe the hyperstoichiometric domain, U_1 and Zr_1 the hypostoichiometric domain. The liquid phase presents a miscibility gap on the uranium–uranium dioxide side at high temperature, which extends into the ternary system.

The ternary oxide solid solution, fcc_C1 (sometimes designated as $(U, Zr)O_{2\pm x}$, fluorite type, or F) was described with a three sublattice model, in agreement with the O–U binary solid solution [12], with the formula: $(U_1, Zr_1)_1(O_1, \square)_2(O_1, \square)_1$. It generates nine binary and quasi-binary interaction parameters, $L(U_1)_1(O_1, \square)_2(\square)_1$, $L(U_1)_1(O_1)_2(O_1, \square)_1$, $L(U_1)_1(O_1, \square)_2(O_1)_1$, $L(U_1)_1(\square)_2(O_1, \square)_1$, $L(Zr_1)_1(O_1, \square)_2(O_1)_1$, $L(Zr_1)_1(O_1, \square)_2(\square)_1$, $L(Zr_1)_1(O_1)_2(O_1, \square)_1$, $L(Zr_1)_1(\square)_2(O_1, \square)_1$, $L(U_1, Zr_1)_1(O_1)_2(\square)_1$ and three ternary ones, $L(U_1, Zr_1)_1(O_1)_2(O_1)_1$, $L(U_1, Zr_1)_1(\square)_2(\square)_1$, $L(U_1, Zr_1)_1(\square)_2(O_1)_1$.

The pseudo-binary tetragonal oxide solid solution, tet_oxide, the ternary metal-oxygen solid solutions, bcc_A2 and hcp_A3, and the intermetallic phase δ were described with a two sublattice model, with the respective formula and associated interaction parameters: tet_oxid: $(U_1, Zr_1)_1(O_1)_2$, quasi-binary $L(U_1, Zr_1)_1(O_1)_2$; bcc_A2: $(O_1, \square)_3(U_1, Zr_1)_1$, three binary $L(O_1, \square)_3(U_1)_1$, $L(O_1, \square)_3(Zr_1)_1$, $L(\square)_3(U_1, Zr_1)_1$ one ternary $L(O_1)_3(U_1, Zr_1)_1$; hcp_A3: $(O_1, \square)_{0.5}(U_1, Zr_1)_1$, three binary $L(O_1, \square_1)_{0.5}(U_1)_1$, $L(O_1, \square_1)_{0.5}(Zr_1)_1$, $L(\square)_{0.5}(U_1, Zr_1)_1$, one ternary $L(O_1)_{0.5}(U_1, Zr_1)_1$; δ: $U_1, Zr_1)_1(Zr_1)_2$, binary, $L(U_1, Zr_1)_1(Zr_1)_2$. The bcc_A2 solid solution presents a miscibility gap at low temperature in the uranium–zirconium system.

The tetragonal and orthorhombic, binary metallic solutions, tet_metal and ort_A20, were described by a simple substitution model, with the formula $(U_1, Zr_1)_1$ and the $L(U_1, Zr_1)_1$ associated interaction parameters.

The values used for the lattice-stabilities of the pure condensed elements have been taken from the SGTE database published by Dinsdale [8], and are reported in Table 1. The thermodynamic data of pure oxides UO_2 and ZrO_2 from the previous assessment [5] are adopted in the present work, Table 2.

The critical assessment of the Gibbs energy coefficients for other binary stoichiometric compounds, and of the excess Gibbs energy interaction parameters for a binary or quasi-binary solution, including the values for metastable structures, was performed by using the optimisation program developed by Lukas et al. [6], which allows to take into account simultaneously all the available experimental information, on equilibrium phase diagram and thermodynamic properties. Assessed Gibbs energy parameters for substance and solution phases are reported in Tables 2 and 3.

For the O–U–Zr ternary system, most of the parameters required by the used models are those of the binary or quasi-binary sub-systems. Only a few ternary interaction parameters have to be evaluated using the Parrot optimisation software included in the Thermocalc computational tool described by Andersson et al. [7], combined with the authors' judgement.

The new set of optimised Gibbs energy parameters of all condensed phases, i.e. lattice-stabilities, pure metallic and oxide substances, solid solutions and liquid phase, will be presented in this work, Tables 1–3. The gas species were taken from the THERMODATA substance database, available in the ThermoSuite software presented by Cheynet et al. [9]. The recent review of oxygen–uranium data presented by Cheynet and Chaud [10] was included. These data are reported in Table 4.

3. Binary and quasi-binary sub-systems

A critical assessment of the binary systems O–U, O–Zr and U–Zr and of the pseudo-binary system O_2U–O_2Zr was previously presented by Chevalier and Fischer [5]. Improvements on all the sub-systems have been made since that time. The phase diagram of each system was calculated by using the re-assessed Gibbs energy parameters for all condensed phases obtained in this work and the available gas phase.

3.1. O–U (oxygen–uranium)

The condensed solutions and stoichiometric substances, with the symbols currently used in this work, are the following: liquid phase, L (metallic, L_1; oxidic, L_2); $UO_{2\pm x}$ solid solution, fcc_C1; O_9U_4(S); O_8U_3(S); O_3U_1(S); U_1(ort_A20); U_1(tet); U_1(bcc_A2).

In our previous work [5], the main experimental incoherency found in this system was the solubility of

Table 1
Gibbs energy parameters (J/g-atom) of condensed pure elements (lattice-stabilities), taken from the SGTE solution database [8]. G(Sub) − G(Ref) = $a_k + b_kT + c_kT\log(T) + d_kT^2 + e_kT^3 + f_kT^{-1} + g_kT^4 + i_kT^7 + j_kT^{-9}$ for $T_k < T < T_{k+1}$. Note: E+ = 10^+; E− = 10^-

Sub	Ref								
T_k	a_k	b_k	c_k	d_k	e_k	f_k	g_k	i_k	j_k
O(L)	O_2(G)								
298.15	−2648.9	+31.44							
U(ort_A20)	SER								
298.15	−8407.734	+130.955 15	−26.9182	+1.251 56E–3	−4.426 05E–6	+38 568			
955	−22 521.8	+292.121 093	−48.66						
U(tet)	SER								
298.15	−5156.136	+106.976 316	−22.841	−1.084 475E–2	+2.7889E–8	+81 944			
941.5	−14 327.309	+244.168 02	−42.9278						
U(bcc_A2)	SER								
298.15	−752.767	+131.5381	−27.5152	−8.355 95E–3	+9.679 07E–7	+204 611			
1049	−4698.365	+202.685 635	−38.2836						
U(L)	SER								
298.15	+3947.766	+120.631 251	−26.9182	+1.251 56E–3	−4.426 05E–6	+38 568			
955	−10 166.3	+281.797 193	−48.66						
Zr(bcc_A2)	SER								
298.15	−525.538 6908	+124.9457	−25.607 406	−3.400 84E–4	−9.728 9735E–9	+25233	−7.614 2894E–11		
2128	−30 705.954 69	+264.284 1628	−42.144						+1.276 057 535E+32
Zr(hcp_A3)	SER								
298.15	−7827.594 691	+125.649 05	−24.1618	−4.377 91E–3		+34 971			
2128	−26 085.920 71	+262.724 1828	−42.144						−1.342 895 52E+31
Zr(L)	SER								
298.15	+10 320.095 31	+116.568 238	−24.1618	−4.377 91E–3		+34 971		+1.627 5E–22	
2128	−8281.259 691	+253.812 609	−42.144						

oxygen in liquid uranium between the temperature of the eutectic reaction, $L_1 \Leftrightarrow UO_{2-x} + U_1$(bcc_A2) and the one of the monotectic reaction, $L_2 \Leftrightarrow UO_{2-x} + L_1$.

These differences have effects on both the liquidus temperatures of U–O alloys on the uranium rich side and the extension of the liquid miscibility gap above the monotectic temperature. A small oxygen solubility is linked to higher liquidus temperatures and a larger miscibility gap, while a high oxygen solubility is linked to lower liquidus temperatures and a smaller miscibility gap in the O–U binary system. It has also a strong influence on the ternary liquidus and liquid miscibility gap.

That is why two different sets of parameters were presented [5], corresponding either to a small solubility of oxygen in uranium and a large miscibility gap, or a higher one and a small miscibility gap. The liquid phase was modelled with an associate model, with the formula $(O_1, O_2U_1, U_1)_1$, and the $UO_{2\pm x}$ solid solution, fcc_C1, by a two sublattice model, with the formula $(O_1, \Box)_2(U_1, \Box)_1$. In this work, the experimental database on oxygen potential and phase diagram was not complete. Moreover, the model used for the fcc_C1 solid solution did not correspond to the real structure. The phase diagram was not calculated with the real gas, but only with diatomic oxygen.

More recently, a progress in the thermodynamic modelling of the O–U binary system was presented by Chevalier et al. [11, 12]. The main improvements were:

- the choice of a small solubility of oxygen in liquid uranium and a wide liquid miscibility gap, in agreement with the recent experimental results concerning a tie line of the liquid miscibility gap by Gueneau et al. [13] in the O–U binary system, and also with the oxygen solubility limit in the (U, Zr, O) liquid determined by Maurisi et al. [14];
- a better description of the UO_{2+x} solid solution, fcc_C1, in agreement with the whole oxygen potential database and the low temperature phase diagram, especially the phase boundaries with O_9U_4(S) and O_8U_3(S). A three sublattice model was used, in better agreement with the real structure of the phase, with the formula $(O_1, \Box)_2(O_1, \Box)_1(U_1)_1$.

Simultaneously, different works on the O–U system were made available, concerning either the oxygen potential database in the hypostoichiometric field by Baichi et al. [15, 16] and in the hyperstoichiometric field by Labroche et al. [17, 18], or the thermodynamic evaluation of the whole system by Gueneau et al. [19]. All these works have been analysed.

The synthesis of the oxygen potential experimental database done by Labroche et al. [17, 18] in the hyperstoichiometry field agrees quite well with and therefore validates our previous work [12]. Moreover, a recent comparison of this work for UO_{2+x} with empirical correlations and

Table 2
Gibbs energy parameters (J/g-atom) of stable condensed substances [5, 12]. G(Sub) − G(Ref) $= a_k + b_kT + c_kT\log(T) + d_kT^2 + e_kT^3 + f_kT^{-1}$ for $T_k < T < T_{k+1}$. Note: E+ $= 10^+$; E− $= 10^-$

Sub	Ref					
T_k	a_k	b_k	c_k	d_k	e_k	f_k
O_2U_1(L)	SER					
298.15	−1.018 368 4975E+6	+4.032 918 1231E+2	−7.465 631 9589E+1	−6.098 470 9916E−3	+1.714 723 93032E−7	+6.491 328 7914E+5
1400	−1.139 083 5289E+6	+1.347 408 7127E+3	−2.052 038 7032E+2	+5.701 393 4304E−2	−5.581 207 6595E−6	+2.170 377 9530E+7
2000	−1.610 016 3643E+6	+4.320 380 3762E+3	−6.022 257 6124E+2	+2.045 824 7891E−1	−1.579 476 7143E−5	+1.254 500 5974E+8
2598	−1.116 005 1467E+6	+8.683 809 1633E+2	−1.309 592 0000E+2	+0.000 000 0000E+0	+0.000 000 0000E+0	+0.000 000 0000E+0
O_2U_1(S)	SER					
298.15	−1.112 057 4111E+6	+4.338 836 4285E+2	−7.465 631 9589E+1	−6.098 470 9916E−3	+1.714 723 9302E−7	+6.491 328 7914E+5
1400	−1.232 772 4425E+6	+1.378 000 5432E+3	−2.052 038 7032E+2	+5.701 393 4304E−2	−5.581 207 6595E−6	+2.170 377 9530E+7
2000	−1.703 705 2778E+6	+4.350 972 2068E+3	−6.022 257 6124E+2	+2.045 824 7891E−1	−1.579 476 7143E−5	+1.254 500 5974E+8
2670	−1.303 384 5812E+6	+1.218 712 2428E+3	−1.670 378 3158E+2	+0.000 000 0000E+0	+0.000 000 0000E+0	+0.000 000 0000E+0
O_3U_1(S)	SER					
298.15	−1.254 274 5343E+6	+5.079 692 7469E+2	−8.870 099 9577E+1	−7.244 799 8863E−3	+0.000 000 0000E+0	+5.045 150 0014E+5
O_8U_3(S)	SER					
298.15	−3.757 004 8974E+6	+3.598 468 0238E+3	−6.116 793 1056E+2	+5.601 275 4009E−1	−1.844 964 0866E−4	+6.125 573 1166E+6
430	−3.713 067 2958E+6	+3.855 550 5193E+3	−6.916 237 4331E+2	+1.028 493 4990E+0	−4.157 854 5194E−4	+0.000 000 0000E+0
466	−2.118 247 1119E+8	+4.093 443 7656E+6	−6.654 670 6062E+5	+9.448 313 7476E+2	−2.516 620 4651E−1	+1.221 599 6790E+10
482.28	+2.376 814 0138E+7	−4.967 879 3874E+5	+7.952 103 4880E+4	−1.031 609 9460E+2	+2.499 984 6914E−2	−1.767 083 0200E+9
520	−1.356 844 4802E+7	+1.788 933 0560E+5	−2.858 898 1158E+4	+3.599 575 5244E+1	−8.591 879 4943E−3	+6.511 329 9440E+8
570	+2.969 687 7315E+7	−5.335 219 3592E+5	+8.342 523 4274E+4	−9.339 440 2393E+1	+1.954 478 2971E−2	−2.493 743 8726E+9
600	−2.372 823 0625E+6	−1.721 505 5510E+4	+2.612 099 9667E+3	−2.869 556 9658E+0	+5.281 323 5444E−4	−1.070 725 4838E+8
700	−4.401 329 9643E+6	+1.183 860 6414E+4	−1.840 068 3712E+3	+1.485 206 4161E+0	−2.725 139 2903E−4	+6.673 037 1801E+7
850.20	−1.298 406 1608E+6	−2.260 866 5240E+4	+3.218 877 0589E+3	−2.302 029 3964E+0	+2.793 841 3576E−4	−2.992 920 6933E+8
1020	−3.658 949 7868E+6	+1.464 782 5563E+3	−2.564 353 1812E+2	−3.056 040 2537E−2	+1.326 558 9540E−6	+9.997 519 6144E+5
O_9U_4(S)	SER					
298.15	−4.571 334 8376E+6	+5.535 224 1533E+2	−1.042 240 0305E+2	−3.179 138 8202E−1	+0.000 000 0000E+0	+0.000 000 0000E+0
315	−2.152 770 7153E+7	+4.626 279 3725E+5	−8.035 313 4511E+4	+1.687 216 0812E+2	−6.686 102 3679E−2	+6.727 317 1549E+8
349.10	+6.826 364 3642E+8	−1.681 367 9498E+7	+2.855 145 3398E+6	−5.273 468 8266E+3	+1.826 222 9613E+0	−3.101 557 9491E+10
358	+8.204 367 2259E+6	−2.954 242 1960E+5	+4.960 774 4082E+4	−8.643 924 0290E+1	+2.805 513 9701E−2	−6.159 312 2338E+8
388	−4.561 894 7011E+6	+7.198 427 1632E+2	−1.396 770 0227E+2	−2.618 065 1252E−1	+5.798 585 0000E−5	−1.519 527 3580E+6
580	−4.620 832 1265E+6	+1.881 865 7690E+3	−3.278 259 2349E+2	−5.746 773 5001E−3	−5.503 398 3333E−6	+1.721 083 1177E+6
1450	+1.000 000 0000E+6	+0.000 000 0000E+0	+0.000 000 0000E+0	+0.000 000 0000E+0	+0.000 000 0000E+0	+0.000 000 0000E+0
O_2Zr_1(fcc_C1)	SER					
298.15	−1.113 681 0000E+6	+4.914 864 3700E+2	−8.000 000 0000E+1			
O_2Zr_1(L)	SER					
298.15	−1.031 671 6200E+6	+3.919 331 0000E+2	−6.962 180 0000E+1	−3.765 600 0000E−3	+0.000 000 0000E+0	+7.029 100 0000E+5
1478	−1.035 025 3400E+6	+4.508 360 9000E+2	−7.810 000 0000E+1			
2208	−1.083 380 5400E+6	+6.413 626 3900E+2	−1.000 000 0000E+2			
O_2Zr_1(monoclinic)	SER					
298.15	−1.126 367 6200E+6	+4.260 761 0000E+2	−6.962 180 0000E+1	−3.765 600 0000E−3	+0.000 000 0000E+0	+7.029 100 0000E+5
O_2Zr_1(tetragonal)	SER					
298.15	−1.121 646 5100E+6	+4.795 157 0300E+2	−7.810 000 0000E+1			

experimental data made by Mason and Mignanelli [20] concluded to its superiority against empirical models commonly used within the nuclear industry, especially for highly oxidizing conditions.

In the hypostoichiometric domain, the recent measurements of the oxygen potential at the two-phase region limits made by Baichi et al. [16] are consistent with our previous work [12]. The only remaining uncertainty is the curvature near the stoichiometry, which is more or less pronounced according to the different authors and modelling.

It was concluded that the modelling represented very satisfactorily the entire oxygen potential database in both single-phase region, UO_{2+x}(fcc_C1), and two-phase regions including other uranium oxides (U_4O_9, U_3O_8, UO_3), the fundamental thermodynamic properties of which having been carefully represented. In the hypostoichiometric domain, our modelling represents the more curved oxygen potential which is naturally compatible with the solidus. A different shape would need more excess interaction parameters, but could be represented if justified by further

Table 3
Excess Gibbs energy parameters of condensed solutions (Φ) and associated metastable reference substances (Sub), assessed in this work. $L_{j,k}\langle\Phi\rangle = \Sigma_\nu L^{(\nu)}_{j,k}\langle\Phi\rangle(y_j - y_k)^\nu L_{j,k:l}\langle\Phi\rangle = \Sigma_\nu L^{(\nu)}_{j,k:l}\langle\Phi\rangle(y_j - y_k)^\nu$. Note: E+ = 10^+; E− = 10^-

Phase	System	Formula	Gibbs energy parameters
Liquid, L		$(O_1, O_2U_1, O_2Zr_1, U_1, Zr_1)_1\langle L\rangle$	
Binary O–U	$L^0(O_1, O_2U_1)_1\langle L\rangle$		$= -71\,931.90$
	$L^0(O_1, U_1)_1\langle L\rangle$		$= 0$
	$L^0(O_2U_1, U_1)_1\langle L\rangle$		$= +98\,284.90 - 24.00559T$
	$L^1(O_2U_1, U_1)_1\langle L\rangle$		$= -68\,039.40$
	$L^2(O_2U_1, U_1)_1\langle L\rangle$		$= -28\,410.34$
Binary O–Zr			
	$L^0(O_1, O_2Zr_1)_1\langle L\rangle$		$= 0$
	$L^0(O_1, Zr_1)_1\langle L\rangle$		$= 0$
	$L^0(O_2Zr_1, Zr_1)_1\langle L\rangle$		$= -23\,653.07$
	$L^1(O_2Zr_1, Zr_1)_1\langle L\rangle$		$= -25\,99.65$
	$L^2(O_2Zr_1, Zr1)_1\langle L\rangle$		$= -36\,782.35$
Binary U–Zr			
	$L^0(U_1, Zr_1)_1\langle L\rangle$		$= 159\,649.67 - 552.638\,89T + 61.636\,215T \log T$
	$L^1(U_1, Zr_1)_1\langle L\rangle$		$= -3067.19$
Quasi-binary O_2U–O_2Zr			
	$L^0(O_2U_1, O_2Zr_1)_1\langle L\rangle$		$= -21\,330.21$
	$L^1(O_2U_1, O_2Zr_1)_1\langle L\rangle$		$= +10\,465.59$
Ternary O–U–Zr			
	$L^0(O_2U_1, Zr_1)_1\langle L\rangle$		$= +33\,190.00$
	$L^1(O_2U_1, Zr_1)_1\langle L\rangle$		$= -75\,000.00$
	$L^2(O_2U_1, Zr_1)_1\langle L\rangle$		$= +31\,100.00$
	$L^0(O_2Zr_1, U_1)_1\langle L\rangle$		$= +33\,190.00$
	$L^1(O_2Zr_1, U_1)_1\langle L\rangle$		$= -110\,000.00$
	$L^2(O_2Zr_1, U_1)_1\langle L\rangle$		$= -160\,000.00$
fcc_C1, (U, Zr)O_{2+x}, fluorite type, F		$(U_1, Zr_1)_1(O_1, \Box)_2(O_1, \Box)_1\langle fcc\_C1\rangle$	
Binary O–U			
	$L^0(U_1)_1(O_1, \Box)_2(O_1)_1\langle fcc\_C1\rangle$		$= 0$
	$L^0(U_1)_1(O_1, \Box)_2(\Box)_1\langle fcc\_C1\rangle$		$= +170\,403.63 - 55.637\,18T$
	$L^0(U_1)_1(O_1)_2(O_1, \Box)_1\langle fcc\_C1\rangle$		$= -237\,337.50 - 51.796\,85T$
	$L^1(U_1)_1(O_1)_2(O_1, \Box)_1\langle fcc\_C1\rangle$		$= -110\,995.28$
	$L^0(U_1)_1(\Box)_2(O_1, \Box)_1\langle fcc\_C1\rangle$		$= 0$
	$G((O_3U_1)(fcc\_C1)) - 1.5G^\circ(O_2(G)) - G^\circ(U_1(ort\_A20))$		$= -1089\,204.89 + 269.063\,81T$
	$G^\circ(U_1(fcc\_C1)) - G^\circ(U_1(ort\_A20))$		$= +50\,000$
	$G(O_1U_1(fcc\_C1)) - 0.5G^\circ(O_2(G)) - G^\circ(U_1(ort\_A20))$		$= +100\,000$
Binary O–Zr			
	$L^0(Zr_1)_1(O_1, \Box)_2(O_1)_1\langle fcc\_C1\rangle$		$= 0$
	$L^0(Zr_1)_1(O_1, \Box)_2(\Box)_1\langle fcc\_C1\rangle$		$= -7357.49$
	$L^1(Zr_1)_1(O_1, \Box)_2(\Box)_1\langle fcc\_C1\rangle$		$= +2107.40$
	$L^0(Zr_1)_1(O_1)_2(O_1, \Box)_1\langle fcc\_C1\rangle$		$= 0$
	$L^0(Zr_1)_1(\Box)_2(O_1, \Box)_1\langle fcc\_C1\rangle$		$= 0$
	$G((O_3Zr_1)(fcc\_C1)) - 1.5G^\circ(O_2(G)) - G^\circ(Zr_1(hcp\_A3)$		$= +200\,000$
	$G^\circ(Zr_1(fcc\_C1)) - G^\circ(Zr_1(hcp\_A3))$		$= +50\,000$
	$G(O_1Zr_1(fcc\_C1)) - 0.5G^\circ(O_2(G)) - G^\circ(Zr_1(hcp\_A3))$		$= +100\,000$
Quasi-binary O_2U–O_2Zr			
	$L^0(U_1, Zr_1)_1(O_1)_2(\Box)_1\langle fcc\_C1\rangle$		$= +80\,798.24 - 28.141\,51T$
	$L^1(U_1, Zr_1)_1(O_1)_2(\Box)_1\langle fcc\_C1\rangle$		$= +5912.99$
Ternary O–U–Zr			
	$L^0(U_1, Zr_1)_1(O_1)_2(O_1)_1\langle fcc\_C1\rangle$		$= 0$

(continued on next page)

Table 3 *(continued)*

Phase	System	Formula	Gibbs energy parameters
	$L^0(U_1, Zr_1)_1(\Box)_2(O_1)_1\langle fcc\_C1\rangle$		$= 0$
	$L^0(U_1, Zr_1)_1(\Box)_2(\Box_1)_1\langle fcc\_C1\rangle$		$= +43\,000.00$
Tetragonal_oxide $(U, Zr)O_2$		$(U_1, Zr_1)_1(O_1)_2\langle tet\_oxide\rangle$	
Quasi-binary O_2U–O_2Zr			
	$L^0(U_1, Zr_1)_1(O_1)_2\langle tet\_oxide\rangle$		$= +78\,793.52 - 23.288\,99T$
	$L^1(U_1, Zr_1)_1(O_1)_2\langle tet\_oxide\rangle$		$= +8492.41$
	$G(O_2U_1(tet\_oxide)) - G(O_2U_1(fcc\_C1))$		$= 1.00T$
hcp-A3		$(U_1, Zr_1)_1(O_1, \Box)_{0.5}\langle hcp\_A3\rangle$	
Binary O–U			
	$L^0(U_1)_1(O_1, \Box)_{0.5}\langle hcp\_A3\rangle$		$= 0$
	$G(O_{0.5}U_1(hcp\_A3)) - 0.25G^\circ(O_2(G))$ $-G^\circ(U_1(ort\_A20))$		$= +100\,000$
Binary O–Zr			
	$L^0(Zr_1)_1(O_1, \Box)_{0.5}\langle hcp\_A3\rangle$		$= -28\,231.33 + 15.269\,92T$
	$L^1(Zr_1)_1(O_1, \Box)_{0.5}\langle hcp\_A3\rangle$		$= -8645.05 + 2.919\,05T$
	$G(O_{0.5}Zr_1(hcp\_A3)) - 0.25G^\circ(O_2(G))$ $-G^\circ(Zr_1(hcp\_A3))$		$= -290\,871.56 + 101.929\,17T$ $-7.139\,787T \log T$
Binary U–Zr			
	$L^0(U_1, Zr_1)_1(\Box)_1\langle hcp\_A3\rangle$		$= -15\,441.71$
	$G(U_1(hcp\_A3)) - G^\circ(U_1(ort\_A20))$		$= +50\,000$
Ternary O–U–Zr			
	$L^0(U_1, Zr_1)_1(O_1)_{0.5}\langle hcp\_A3\rangle$		$= -255\,000$
bcc_A2		$(U_1, Zr_1)_1(O_1, \Box)_3\langle bcc\_A2\rangle$	
Binary O–U			
	$L^0(U_1)_1(O_1, \Box)_3\langle bcc\_A2\rangle$		$= 0$
	$G(O_3U_1(bcc\_A2))$–H_{SER}		$= -272\,189.68 + 507.835\,04T - 88.701T \log T$ $-7.2448\text{E}{-3}T^2 + 5.045\,16\text{E}{+5}T^{-1}$
Binary O–Zr			
	$L^0(Zr_1)_1(O_1, \Box)_3\langle bcc\_A2\rangle$		$= -747\,917.32 + 137.655\,78T$
	$G(O_3Zr_1(bcc\_A2)) - 1.5G^\circ(O_2(G))$ $-G^\circ(Zr_1(bcc\_A2))$		$= -978\,407.6 + 332.0716T - 18.267\,556T \log T$ $+1.160\,192\text{E}{-3}T^2 + 6.4\text{E}{-8}T^3$ $+7.825\text{E}{+5}T^{-1}$
Binary U–Zr			
	$L^0(U_1, Zr_1)_1(\Box)_3\langle bcc\_A2\rangle$		$= +60\,574.02 - 221.453\,71T$ $+24.779\,079T \log T$
	$L^1(U_1, Zr_1)_1(\Box)_3\langle bcc\_A2\rangle$		$= +8418.51$
	$L^2(U_1, Zr_1)_1(\Box)_3\langle bcc\_A2\rangle$		$= +512.70$
	$L^3(U_1, Zr_1)_1(\Box)_3\langle bcc\_A2\rangle$		$= +3700.10$
	$L^4(U_1, Zr_1)_1(\Box)_3\langle bcc\_A2\rangle$		$= +5860.56$
Ternary O–U–Zr			
	$L^0(U_1, Zr_1)_1(O_1)_3\langle bcc\_A2\rangle$		$= -255\,010$
Tetragonal_metal		$(U_1, Zr_1)_1(\Box)_1\langle tet\_metal\rangle$	
Binary U–Zr			
	$L^0(U_1, Zr_1)_1(\Box)_1\langle tet\_metal\rangle$		$= -2580.13$
	$G(Zr_1(tet\_metal)) - G^\circ(Zr_1(hcp\_A3))$		$= +35\,000$
ort_A20		$(U_1, Zr_1)_1(\Box)_1\langle ort\_A20\rangle$	
Binary U–Zr			
	$L^0(U_1, Zr_1)_1(\Box)_1\langle ort\_A20\rangle$		$= -2843.69$
	$G(Zr_1(ort\_A20)) - G^\circ(Zr_1(hcp\_A3))$		$= +38\,000$
δ		$(U_1, Zr_1)_2(Zr_1)1\langle\delta\rangle$	
Binary U–Zr			
	$L^0(U_1, Zr_1)_2(Zr_1)_1\langle\delta\rangle$		$= 0$
	$G(U_2Zr_1(\delta)) - 2G^\circ(U_1(ort\_A20))$ $-G^\circ(Zr_1(hcp\_A3))$		$= +8.062\,86T$
	$G(Zr_3(\delta)) - 3G^\circ(Zr_1(hcp\_A3))$		$= +6.414\,87T$

Table 4
Gibbs energy parameters (J/g-atom) of gaseous species [9, 10]. G(Sub) − G(Ref) = $a_k + b_kT + c_kT\log(T) + d_kT^2 + e_kT^3 + f_kT^{-1}$ for $T_k < T < T_{k+1}$. Note: E+ = 10^+; E− = 10^-

Substance T_k	T_{max} a_k	b_k	c_k	d_k	e_k	f_k
O_1(G)	20 000.00					
298.15	+2.431 527 1223E+5	−1.976 835 3956E+1	−2.118 778 9894E+1	+3.119 265 7423E−4	−4.474 310 9082E−8	−3.942 921 4725E+4
1200.00	+2.427 757 5832E+5	−1.802 978 1131E+1	−2.139 357 1775E+1	+2.630 740 3526E−4	−2.101 874 7482E−8	+4.556 641 8264E+4
4200.00	+2.561 532 6700E+5	−6.266 080 1072E+1	−1.595 823 0064E+1	−7.223 247 1677E−4	+1.250 209 9791E−8	−6.179 930 6436E+6
8600.00	+1.960 061 9753E+5	+3.366 632 8610E+1	−2.662 230 2213E+1	+1.349 779 7312E−4	−6.538 466 4400E−10	+5.877 72 39294E+7
O_2(G)	20 000.00					
298.15	−7.060 288 2651E+3	−4.915 283 2099E+1	−2.258 829 6136E+1	−9.794 796 0689E−3	+1.235 305 9908E−6	−7.150 011 5612E+4
1100.00	−1.308 300 1915E+4	+2.507 161 6144E+1	−3.361 548 6270E+1	−1.181 363 6232E−3	+1.163 439 6981E−8	+5.102 040 7218E+5
3500.00	+1.337 305 5271E+4	−4.996 678 7673E+1	−2.465 239 1914E+1	−2.619 171 7530E−3	+5.989 633 7111E−8	−1.446 964 7464E+7
8600.00	−3.961 063 4669E+5	+6.091 001 0981E+2	−9.753 685 1127E+1	+3.108 200 0140E−3	−2.395 161 6364E−8	+4.138 339 2011E+8
17 000.00	−1.460 957 1329E+5	+3.437 604 9822E+2	−6.965 034 8186E+1	+1.748 841 6266E−3	−1.172 809 5723E−8	+0.000 000 0000E+0
O_3(G)	6000.00					
298.15	+1.318 440 1713E+5	−6.199 324 3331E+1	−2.363 802 9683E+1	−3.329 796 5924E−2	+6.046 879 1438E−6	+4.007 225 2494E+4
700.00	+1.152 896 3785E+5	+1.710 291 1110E+2	−5.929 252 3898E+1	+1.540 008 2084E−3	−4.581 898 6202E−7	+1.511 599 4127E+6
1400.00	+5.722 063 5930E+4	+6.570 720 8335E+2	−1.272 032 3834E+2	+3.680 294 8955E−2	−3.886 811 0847E−6	+1.081 676 4021E+7
2300.00	+1.148 003 4113E+6	−4.854 521 9108E+3	+5.851 218 2213E+2	−1.707 131 5510E−1	+7.489 946 4204E−6	−3.035 395 4198E+8
3400.00	−1.911 361 5418E+6	+6.239 759 4274E+3	−7.815 266 8489E+2	+1.012 566 0312E−1	−2.680 985 0377E−6	+9.837 240 1000E+8
4900.00	−2.306 880 2126E+5	+1.686 540 1835E+3	−2.427 144 5722E+2	+2.443 780 7370E−2	−6.265 991 6640E−7	+0.000 000 0000E+0
O_1U_1(G)	6000.00					
298.15	+8.509 202 1960E+3	−5.690 015 1336E+1	−2.837 625 2134E+1	−7.953 290 2671E−3	+1.337 413 5150E−6	+5.878 258 5000E+4
900.00	+3.884 735 3654E+3	+2.491 448 4585E+0	−3.732 824 6151E+1	−1.681 712 3555E−5	+5.640 917 6273E−10	+5.29 972 63600E+5
O_2U_1(G)	6000.00					
298.15	−5.026 672 8973E+5	−3.661 268 5831E+1	−3.504 369 8847E+1	−2.305 528 3480E−2	+4.478 371 5890E−6	+1.310 270 2243E+5
700.00	−5.127 229 6825E+5	+1.089 488 9217E+2	−5.744 862 1618E+1	−2.194 671 1760E−4	+1.138 453 1507E−8	+1.005 127 3366E+6
3700.00	−5.118 333 3989E+5	+1.104 903 7488E+2	−5.771 995 3600E+1	−3.659 159 0400E−5	+0.000 000 0000E+0	+0.000 000 0000E+0
O_3U_1(G)	6000.00					
298.15	−8.220 749 3375E+5	+1.346 959 6388E+2	−6.440 854 5252E+1	−1.588 970 0244E−2	+2.537 476 8887E−6	+3.568 197 5451E+5
1000.00	−8.317 187 9176E+5	+2.631 256 4731E+2	−8.375 909 1680E+1	+7.396 988 4218E−4	−6.639 341 2901E−8	+1.214 304 7874E+6
1600.00	−8.308 331 9874E+5	+2.559 094 5704E+2	−8.274 517 0917E+1	+1.735 368 4872E−4	−5.688 741 0089E−9	+1.041 983 3231E+6
O_1Zr_1(G)	4500.00					
298.15	+7.862 533 5513E+4	−2.196 140 1511E+2	+4.879 074 5312E+0	−8.011 928 5250E−2	+2.044 475 0458E−5	−1.056 960 4231E+5
700.00	+4.980 213 2367E+4	+3.074 674 8259E+2	−7.912 448 5486E+1	+2.295 609 7158E−2	−2.419 327 9877E−6	+1.589 315 7028E+6
1400.00	+8.385 975 9894E+4	+1.146 276 5307E+1	−3.748 087 3659E+1	+1.787 266 8682E−4	−7.847 280 5589E−8	−3.698 206 9940E+6
O_2Zr_1(G)	4500.00					
298.15	−4.144 014 6958E+5	+3.150 719 4444E+1	−4.267 286 7877E+1	−1.241 760 6322E−2	+1.857 615 4371E−6	+2.945 175 4856E+5
1100.00	−4.294 868 3328E+5	+1.820 026 7562E+2	−6.447 947 7978E+1	+2.737 681 0723E−3	−2.201 940 0392E−7	+2.442 191 4278E+6
U_1(G)	6000.00					
298.15	+5.595 197 5434E+5	−2.212 866 3062E+0	−3.260 704 6251E+1	+1.136 643 7766E−2	−2.449 181 0700E−6	+1.530 094 0077E+5
1000.00	+5.800 965 8408E+5	−2.096 754 4463E+2	−2.661 589 2917E+0	−8.401 472 0765E−3	+4.952 459 9130E−8	−2.547 926 2437E+6
2300.00	+6.530 073 0689E+5	−5.730 712 1546E+2	+4.424 062 3227E+1	−2.198 625 5660E−2	+7.969 465 2619E−7	−2.406 600 6341E+7
4300.00	+6.935 462 0964E+4	+1.107 370 4312E+3	−1.563 451 0622E+2	+8.876 606 4166E−3	−1.001 102 9279E−7	+2.965 931 1222E+8
6800.00	+1.375 518 1202E+5	+1.032 777 0752E+3	−1.487 771 4168E+2	+8.932 833 4071E−3	−1.170 165 4550E−7	+2.123 858 9076E+8
9800.00	+1.245 144 0404E+6	−4.962 250 7344E+2	+1.733 530 3565E+1	−2.272 445 8243E−03	+2.645 223 5804E−8	−1.187 945 6346E+9
Zr_1(G)	10 000.00					
298.15	+5.744 919 1494E+5	+8.210 414 9638E+1	−3.869 111 0000E+1	+1.152 846 0000E−2	−1.693 255 0000E−6	+2.706 388 0000E+5
700.00	+5.836 053 6701E+5	−1.836 602 0705E+1	−2.406 106 0000E+1	+1.743 641 0000E−3	−5.943 123 3333E−7	−7.489 475 0000E+5
1300.00	+5.814 567 4711E+5	−3.833 342 4969E+1	−2.046 361 0000E+1	−2.961 084 0000E−3	+1.083 914 3333E−7	+5.263 525 0000E+5
2700.00	+6.183 601 2548E+5	−1.542 783 4040E+2	−6.647 343 0000E+0	−4.673 895 5000E−3	+1.068 335 8333E−7	−1.587 234 0000E+7
6600.00	+4.918 753 4554E+5	+1.395 008 5082E+2	−4.068 801 0000E+1	−6.383 570 0000E−4	+1.791 253 3333E−8	+7.149 695 0000E+7
Zr_2(G)	6000.00					
298.15	+9.022 786 7567E+5	+4.044 861 3064E+1	−3.713 672 0000E+1	−3.203 965 5000E−4	−4.306 051 6667E−9	+8.542 215 0000E+4
3600.00	+8.836 325 7030E+5	+6.420 986 7372E+1	−3.933 356 0000E+1	−1.019 669 0000E−3	+6.097 996 6667E−8	+1.406 580 5000E+7

analysis. In any case, it does not affect the calculation of phase equilibria, because the limit conditions are respected.

The comparison of the two assessment works of Chevalier et al. [11, 12], and Gueneau et al. [19] still showed some differences on the calculated phase diagram. Two points have been found to be subject to discussion:

- in the hypostoichiometry field, the shape of the miscibility gap, which may exist up to vaporisation [11] or be closed before [12, 19];
- in the hyperstoichiometry field, the temperature of the invariant reaction $L_2 \Leftrightarrow UO_{2+x} + G$ at a total pressure of 1 atmosphere, varying between about 2700 K [19], and 3073 K [12]. This temperature was quoted in dashed points by Levinskii [21] in the compilation "phase diagrams for ceramists" as 2873 K.

That's why the O–U binary system has been re-assessed in this study, on the basis of the selected models [12] and of specific choices for the shape of the liquid miscibility gap in the hypostoichiometric field, and for the temperature of the invariant reaction at 1 atmosphere in the hyperstoichiometric field.

The calculated O–U phase diagram is presented with special points and invariant reactions, and compared to some selected experimental points [22–34] on Fig. 1(a). Different enlargments have been previously presented [12]; an enlargement of the oxide part is presented on Fig. 1(b).

3.2. O–Zr (oxygen–zirconium)

The condensed solutions and stoichiometric compounds, with the symbols currently used in this work, are the following: liquid phase, L; ZrO_{2-x} solid solution, fcc_C1; O_2Zr_1(tet), tetragonal; O_2Zr_1(mon), monoclinic; Zr_1(hcp_A3); Zr_1(bcc_A2).

In our previous work [5], the oxygen potential database was not complete, and some disagreements were found between the calculated and experimental phase diagram, especially concerning the phase boundaries of the two-phase regions hcp_A3 + O_2Zr_1(mon, tet) at low temperature and hcp_A3 + bcc_A2. Moreover, no experimental liquidus was available at high temperature for the two-phase region L + ZrO_{2-x}(fcc_C1).

In this work, the bibliography has been updated, and the complete list including new references is given [35–50].

The O–Zr system has been re-assessed in this work, by taking into account the complete oxygen potential and phase diagram database. The liquid phase was modelled with an associate model, with the formula (O_1, O_2Zr_1, Zr_1), and the fcc_C1, hcp_A3 and bcc_A2 solid solutions by a two sublattice model, with the formula, $(Zr_1)_1(O_1, \square)_2(O_1, \square)_1$, $(O_1, \square)_{0.5}(Zr_1)_1$, $(O_1, \square)_3(Zr_1)_1$, respectively. The calculated O–Zr phase diagram is presented with special points and invariant reactions, and compared to some selected experimental points [35, 37–39, 42, 43, 48] on Fig. 2.

The agreement between the calculated and experimental phase boundaries has been improved. Two other assessments were made by Liang et al. [49] and Arroyave et al. [50]. The main differences between our work and the two others are the inclusion of several stoichiometric oxides in the zirconium rich domain by [49, 50], at low temperature ($T < 750$ K), which do not interest severe accidents, and the shape of the liquidus at high temperature, more or less curved, which is important for the extension of the O–U liquid miscibility gap in the O–U–Zr ternary system at high zirconium content. The low temperature oxides will be included in the future, but new experimental measurements would be necessary to validate the liquidus shape at high temperature.

3.3. U–Zr (uranium–zirconium)

The condensed solutions and stoichiometric compounds, with the symbols currently used in this work, are the following: liquid phase, L; body centred cubic solid solution, bcc_A2; tetragonal uranium rich solid solution, tet_metal; orthorhombic uranium rich solid solution, ort_A20; hexagonal close packed zirconium rich solid solution, hcp_A3; intermetallic phase δ.

In our previous work [5], the non-stoichiometric range of the intermetallic phase δ was not represented, as it was considered as a stoichimetric compound, U_3Zr_7(S). Moreover, incoherencies were found between the experimental activities in the bcc_A2 solid and liquid solutions, which show a strongly negative deviation from ideality in the temperature range 1723–1873 K [51, 52] and the existence of a miscibility gap in the bcc_A2 solid solution at low temperature, indicating a positive deviation from ideality. Even though no new recent experimental value is available for this system, these two points justified a re-assessment of the system. Moreover, the two existing assessments, by Leibowitz et al. [53] and Ogawa and Iwai [54], show an unrealistic excess Gibbs energy of the liquid phase, which becomes more and more negative above about 1600 K, especially in the second case [54].

These are the reasons why a new critical assessment is presented in this work, which takes into account the non-stoichiometry range of the intermetallic phase δ and proposes more realistic excess Gibbs energies for the liquid and bcc_A2 solid solutions. The liquid phase, L, and the solid solutions, bcc_A2, tet_metal, ort_A20 and hcp_A3, have been modelled with a simple substitutional model, with the formula $(U_1, Zr_1)_1$. The intermetallic phase δ has been represented with a two sublattice model, with the formula $(U_1, Zr_1)_2(Zr_1)_1$, which allowed us to represent the non-stoichiometry range. The calculated U–Zr phase diagram is presented on Fig. 3(a) and (b) with special points and invariant reactions, and compared to some selected

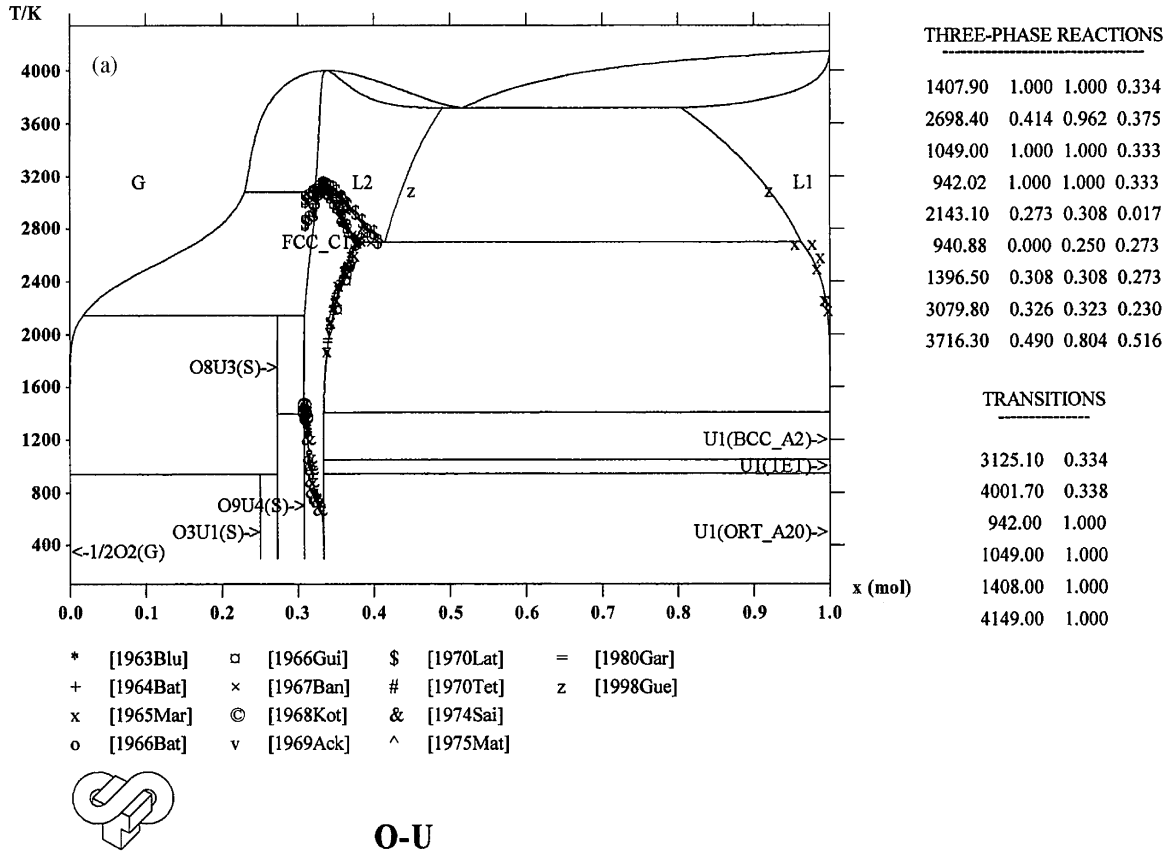

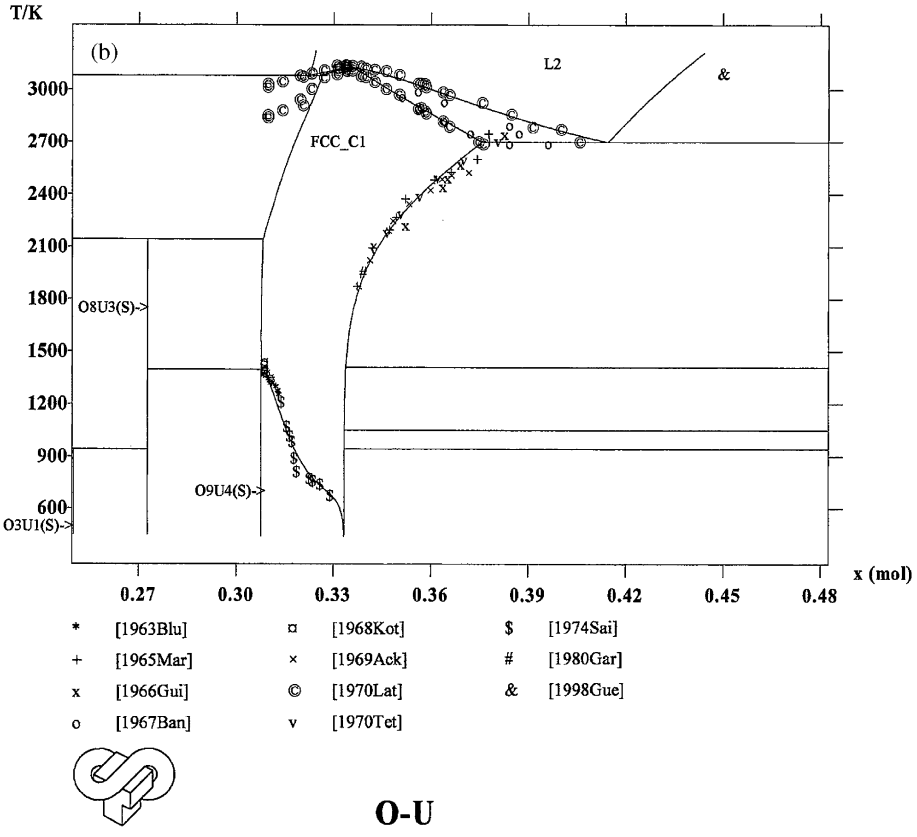

Fig. 1. Calculated O–U equilibrium phase diagram compared to some of the selected experimental points: (a) global, (b) enlargement of the oxide part.

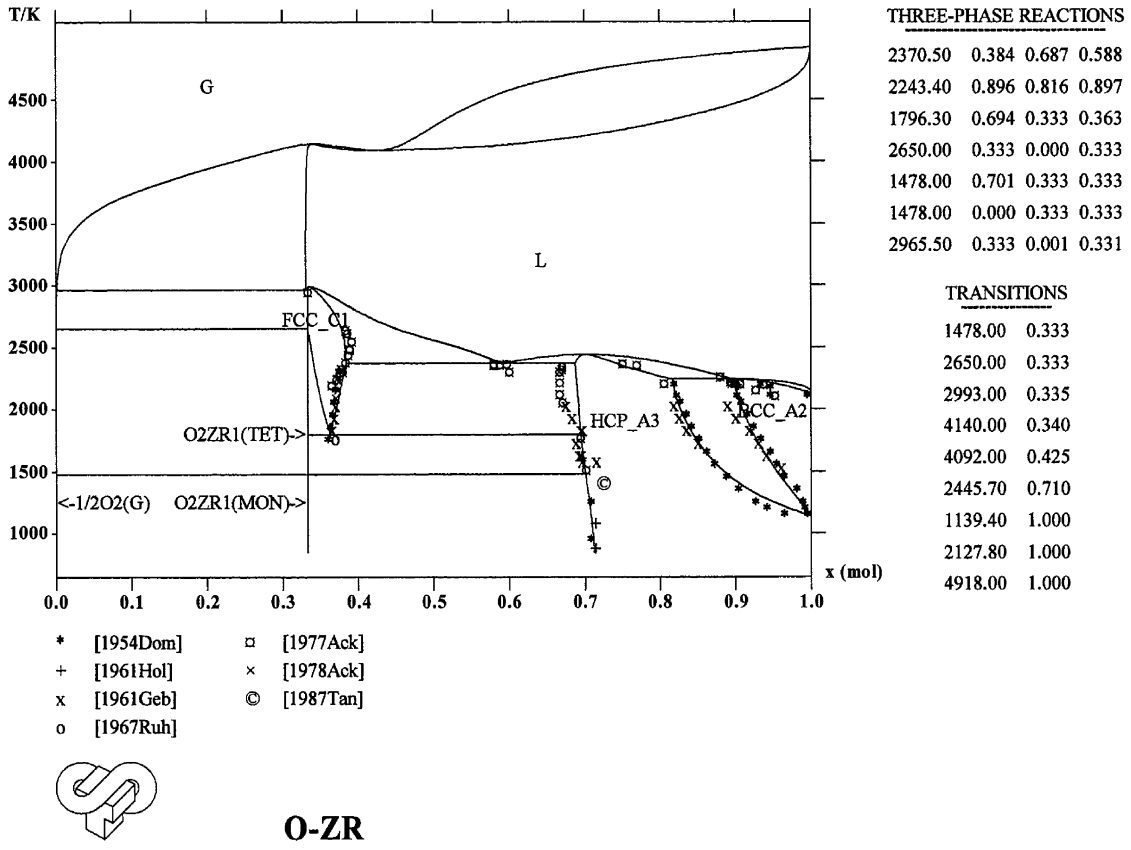

Fig. 2. Calculated O–Zr equilibrium phase diagram compared to the selected experimental points.

experimental points taken from the open literature [52–62]. The agreement is quite satisfactory. The activity of uranium is in agreement with the experimental ones of Maeda et al. [52].

However, further work should be made for evaluating the quality of the extrapolation of the excess Gibbs energy of the liquid phase at temperatures well above the liquidus, in the domain of interest for severe nuclear accidents, up to 3500 K. The data of Kanno et al. [51] were found to be too negative, probably for experimental reasons (tantalum Knudsen cell, oxygen impurities).

3.4. O_2U_1–O_2Zr_1 (uranium dioxide–zirconium dioxide)

The condensed solutions and stoichiometric compounds, with the symbols currently used in this work, are the following: liquid phase, L; $(U, Zr)O_2$ solid solution, fcc_C1; $(U, Zr)O_2$ solid solution, tet_oxide; O_2Zr_1(mon), monoclinic.

The assessment of the O_2U_1–O_2Zr_1 quasi-binary system was initiated in 1990 by Relave et al. [63], as a preliminary step for the thermodynamical calculation of phase equilibria in a quinary oxide system of first interest in nuclear energy field: UO_2–ZrO_2–SiO_2–CaO–Al_2O_3, such as liquidus and solidus temperatures of some selected core (UO_2–ZrO_2)–concrete (Al_2O_3–CaO–SiO_2) mixtures [64]. This basic system was a beginning in the cooperative development of the nuclear thermodynamic database with the United Kingdom [65]. A thermodynamic assessment of this system was made by Yashima et al. [66].

However, new experimental points have been made available by the recent works of Punni and Mignanelli [67], giving information on solidus and liquidus temperatures of uranium–zirconium oxides, and also of Baichi et al. [15, 68] giving activity of UO_2 in the solid solution in a wide range of temperature (2000–2500 K). The list of bibliographic references has been updated: [69–78].

The O_2U_1–O_2Zr_1 quasi-binary system was re-assessed in the framework of the ENTHALPY project [4] and improved in this work. The liquid phase was described with a simple substitutional model, with the formula $(O_2U_1, O_2Zr_1)_1$, while the two solid solutions fcc_C1 and tet_oxide were described by a two sublattice model, with the formula $(U_1, Zr_1)_1(O_1)_2$.

The critical analysis of the pseudo-binary system O_2U_1–O_2Zr_1 has been made by Baichi [15]. This work, combined with new available experimental data [67, 68], allowed us to obtain a satisfactory agreement with the selected experimental points for the calculated phase diagram (without deviation from stoichiometry) and for the activity of UO_2 in the fcc_C1 solid solution. The O_2U_1–O_2Zr_1 quasi-binary phase diagram is presented with special points and invariant reactions on Fig. 4.

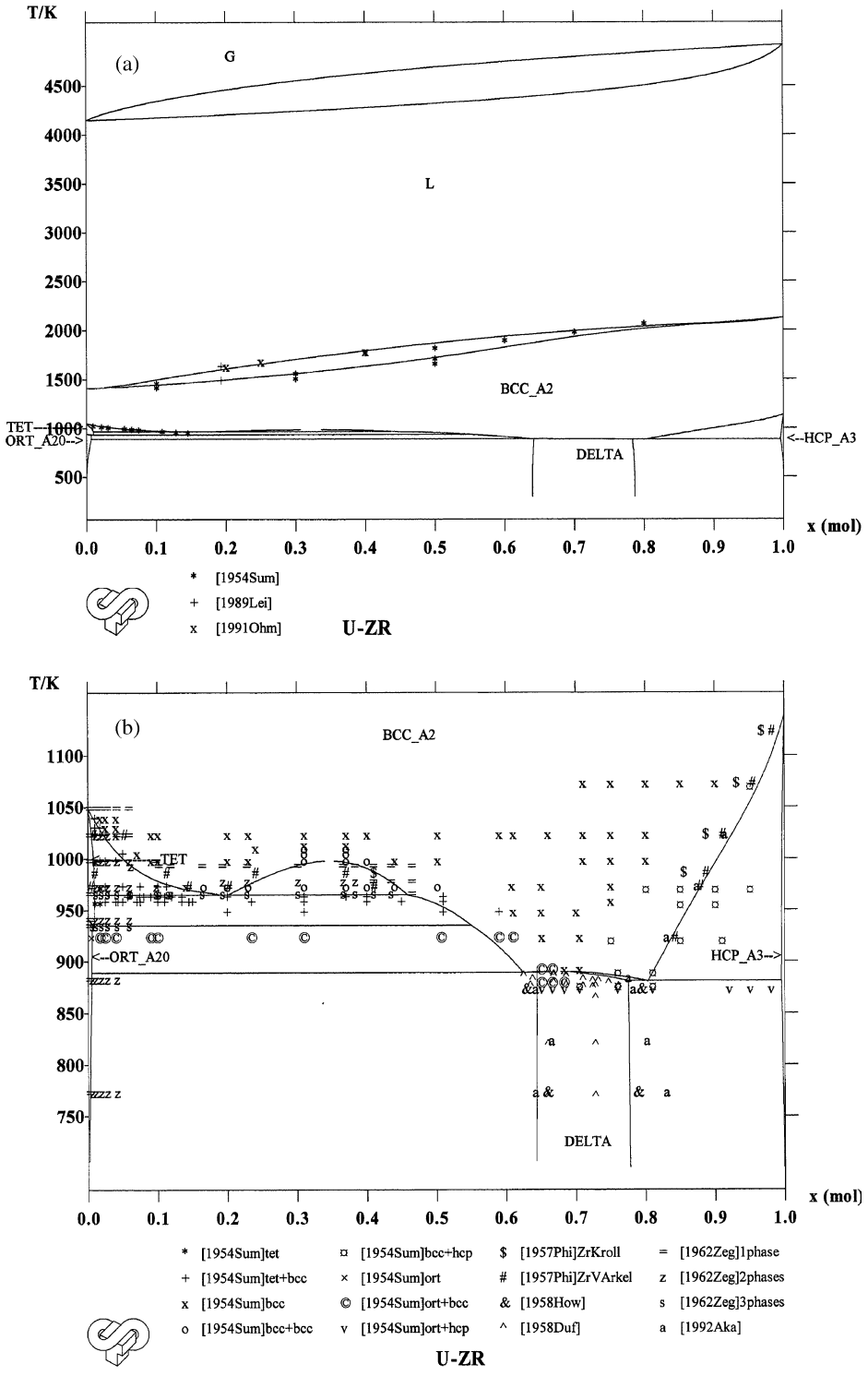

Fig. 3. Calculated U–Zr equilibrium phase diagram compared to the selected experimental points: (a) with the gas phase, (b) in the solid state.

4. Ternary system

4.1. Short presentation of the different phases

The different possible condensed phases resulting from the analysis of the O–U, O–Zr and U–Zr, binary, or O_2U–O_2Zr pseudo-binary sub-systems, and also from all the available experimental information, are the following: the ternary liquid phase, L, may present a miscibility gap on the uranium–uranium dioxide side at high temperature, which extends in the ternary system (metallic, L_1; oxidic, L_2); the ternary intermediate oxide cubic face centred solid

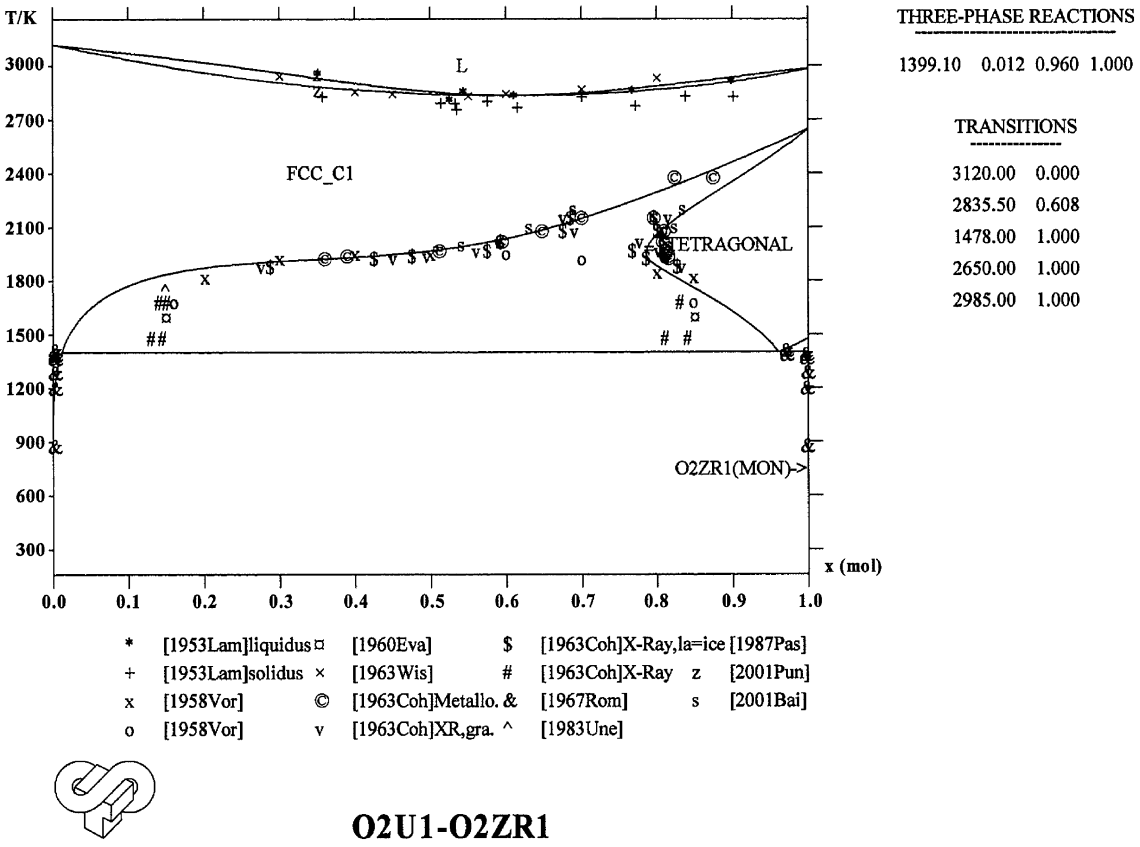

Fig. 4. Calculated O_2U–O_2Zr equilibrium phase diagram compared to the available experimental points.

solution, fcc_C1, fluorite type, $(U, Zr)O_{2\pm x}$, F; the ternary intermediate oxide tetragonal solid solution, tet_oxide, $(U, Zr)O_2$, T; the ternary terminal metallic body centred cubic solid solution, bcc_A2, which may dissolve 10 at.% O at maximum on the zirconium rich side (uranium and zirconium form a continuous solid solution at high temperature and a miscibility gap at lower temperature), B; the ternary terminal metallic hexagonal close packed solid solution, hcp_A3, which may dissolve 35 at.% O at maximum on the zirconium rich side and has a very limited uranium content (about 2 or 3 at.%), H; the binary terminal uranium rich tetragonal solid solution, tet_metal, with a very limited zirconium content; the binary terminal uranium rich orthogonal solid solution, ort_A20, with a negligible zirconium content; the pure oxides U_3O_8(S), U_4O_9(S), UO_3(S) and ZrO_2(monoclinic), all considered as stoichiometric; the intermediate metallic phase, δ, with a non-stoichiometry range.

4.2. Experimental information

A first compilation of the experimental equilibria in the O–U–Zr ternary system has been presented in detail by Chevalier and Fischer [5], reassembling the following results:

- Saller et al. [79]: isothermal section at $T = 1368$ K, with experimental points in the diphasic fcc_C1 + hcp_A3, fcc_C1 + bcc_A2 and triphasic fcc_C1 + hcp_A3 + bcc_A2 domains;
- Junke and White [80]: “tentative” Zr–UO_2 isopleth;
- Politis [81]: compilation of the binary U–Zr, Zr–ZrO_2, U–O, U–UO_2 and pseudo-binary UO_2–ZrO_2 subsystems; topology of the isothermal sections at $T = 1273$ and 1773 K; experimental points in the $(U, Zr)O_{2-x}$ + L two-phase region at $T = 2273$ K; pseudo-binary α-Zr(O)–UO_2 section, the true composition of the left side being not clear and supposed by Hagrman et al. [82] to be oxygen stabilised α phase zirconium, $ZrO_{0.43}$, showing a miscibility gap, with experimental points in the L_1 and $(U, Zr)O_{2-x}$ monophasic, α-Zr(O) + UO_{2-x}, L_1 + $(U, Zr)O_{2-x}$, $L_1 + L_2$, $L_2 + (U, Zr)O_{2-x}$ two-phase regions, monotectic reaction $L_2 \Leftrightarrow L_1 + (U, Zr)O_{2-x}$ at $T = 2673$ K, eutectic one $L_1 \Leftrightarrow \alpha$–Zr(O) + UO_2 around $T = 2113$ K;
- Hofman et al. [83], Hofman and Politis [84]: compilation of the isothermal sections at $T = 1273$, 1773 and 2273 K; pseudo-binary α-Zr(O)–UO_2 sections similarly to [81]; onset of melting of a number of O–U–Zr compositions;
- Skokan [85]: revised α-Zr(O)–UO_2 isopleth, left side $ZrO_{0.43}$, eutectic at $T = 2173$ K, liquidus shifted to

higher UO_2 content, with experimental points in the α-Zr(O) + (U, Zr)O_{2-x}, α-Zr(O) + L_1, L_1 + (U, Zr)O_{2-x}; hypothetical sections at $T = 1873$ and 2073 K;
- Yamanaka et al. [86]: tentative isothermal section at $T = 1273$ K, with experimental points on the line UO_2–Zr in the diphasic and triphasic domains, fcc_C1 + O_2Zr_1(mon) + hcp_A3, fcc_C1 + hcp_A3, fcc_C1 + hcp_A3 + bcc_A2, hcp_A3 + bcc_A2;
- Yamanaka et al. [87]: isothermal section at $T = 1673$ K, with the diphasic and triphasic domains fcc_C1 + tet_oxide, fcc_C1 + tet_oxide + hcp_A3, fcc_C1+hcp_A3, fcc_C1+hcp_A3+L_1, fcc_C1+L_1, hcp_A3 + L_1, hcp_A3 + L_1 + bcc_A2, hcp_A3 + bcc_A2; topology identical to Politis and Hofman [81, 83, 84] at 1773 K; small solubility of uranium in α-Zr(O);
- Miyake et al. [88]: isothermal sections at $T = 1273$ and 1673 K, identical to Yamanaka et al. [86, 87];
- Hofmann et al. [89]: new compilation of Zr–ZrO_2, O–U–Zr at $T = 1773$, 1873, 2073 and 2273 K, α-Zr(O)–UO_2 re-actualised from Skokan [85];
- Hayward and George [90, 91]: solubility of UO_2 in Zr and $ZrO_{0.43}$ over the temperature range 2273–2773 K; UO_{2-x}–$ZrO_{0.54}$ vertical section, without miscibility gap;
- Maurisi et al. [14]: oxygen solubility limit in the (U, Zr, O) liquid in the range 2020–2320 K for U/Zr = 1.5.

Since this work, further measurements have been made, and new experimental results are now available:

- Gueneau et al. [13]: liquid miscibility gap: O–U: $T = 3090 \pm 100$ K, L_2: $x_O = 0.55 \pm 0.02$, $x_U = 0.45 \pm 0.02$, L_1: $x_O = 0.02 \pm 0.02$, $x_U = 0.98 \pm 0.02$; O–U–Zr: $T = 3223 \pm 100$ K, L_1: $x_O = 0.16 \pm 0.04$, $x_U = 0.44 \pm 0.02$, $x_{Zr} = 0.40 \pm 0.02$, L_2: $x_O = 0.48 \pm 0.04$, $x_U = 0.29 \pm 0.02$, $x_{Zr} = 0.23 \pm 0.02$;
- Farmer et al. [92]: DTA determination of liquidus and solidus temperatures of six specific corium compositions, representative of PWR (pressurised water reactors) and BWR (water reactors) configurations in different states of oxidation; x_O, x_U, x_{Zr}, T^L, T^S reported in Table 5 (given in Appendix);
- Punni and Mignanelli [67]: solidus and liquidus temperatures of overstoichiometric uranium–zirconium dioxides; $U_{0.65}Zr_{0.35}O_{2.000}$, $T^L = 2951$ K, $T^S = 2863$ K; $U_{0.65}Zr_{0.35}O_{2.052}$, $T^L = 2911$ K, $T^S = 2823$ K; $U_{0.65}Zr_{0.35}O_{2.098}$, $T^L = 2834$ K, $T^S = 2755$ K.

4.3. Critical analysis of main incoherencies in the experimental information

In analysing the available experimental information, some features of the phase diagram appeared to be subject to controversy, especially at temperatures interesting hypothetical severe accidents, above 2000 K.

4.3.1. Apparent contradictions in the previous experimental works

A lot of apparent contradictions have been found for the vertical sections of interest, α-Zr(O)–UO_2.

First of all, the left side of the diagram, {ZrO_xT^f(K)}, varied with the different authors, successively as: {0, 2125 K} [80], {0.51?, 2144 K} [81], {0.51?, 2228 K} [83], {0.43, 2493 K} [82], {0.43, 2273 K} [85, 89], {0.54, 2323–2353 K} [91]. In the section revised by Skokan [85], the oxygen concentration in α-Zr(O) was fixed at 30 at.% instead of 34 at.% by Politis [81]. Except for Junke and White [80], who studied the vertical section Zr–UO_2, and thus indicated the true melting point of Zr, assessed as 2128 K [8], the left side of the diagram should correspond to the oxygen saturated hcp_A3 solid solution in the O–Zr binary system, varying from {0.43, <2148 K} according to Domagala and McPherson [35] to {0.43, <2403 K} according to Ackermann et al. [42]. This point has already been clarified in the re-assessment of the O–Zr binary system, in which Ackermann et al.'s diagram was selected. Consequently, the calculated melting temperature of $ZrO_{0.43}$ or $O_{0.3}Zr_{0.7}$ is equal to 2413 K, and thus, the selected left side for α-Zr(O) is {0.43, 2413 K}, located between the values given by Hagrman et al. [82] and Hayward and George [91], and in contradiction with others [81, 83, 85, 89].

Secondly, differences have been found concerning the eutectic temperature L $\Leftrightarrow$ fcc_C1 + hcp_A3 in the α-Zr(O)–UO_2 vertical section, determined as 2113 K by Politis [81] and Hofman and Politis [84], and as 2173 K by Skokan [85]. In fact, on a theoretical point of view, this temperature is not constant in a ternary system, and the L + fcc_C1 + hcp_A3 domain may exist over a wide temperature range in the O–U–Zr ternary system, decreasing when the UO_2 content increases. This feature will explicitly appear in this work in the calculated $ZrO_{0.43}$–UO_2 vertical section.

Third, there is a noticeable inconsistency between the isothermal section at 2273 K reported by Politis [81] and Hofman and Politis [84], and the $ZrO_{0.43}$–UO_2 vertical section reported by the same authors [81, 83]. The isothermal section gives experimental compositions located either in the two-phase field L + (U, Zr)O_{2-x}, or in the monophasic liquid region, and allows to estimate the phase boundary L/L + (U, Zr)O_{2-x} at high zirconium content. At $T = 2273$ K, the solubility limit is estimated to be 14 mol% UO_2 from the isothermal section, whereas it is equal to 8 mol% UO_2 from the vertical section. The limit of solubility was determined in the temperature range 2073–2573 K. In the revised vertical section proposed by Skokan [85], the maximum amount of UO_2 which can be dissolved at 2273 K is about 16 mol%, which agrees significantly better with the isothermal section (14 mol%) than the earlier value of 8 mol%. The limit of solubility of UO_2 in $ZrO_{0.43}$ has been determined in the range 1873–2373 K. The new vertical section was included in the more recent compilation work of Hofman et al. [89]. In this work, the liquidus line of

the two-phase field $(U, Zr)O_{2-x}$ + L on the Zr-rich side is shifted to higher UO_2 contents. In a general way, the limit of solubility of oxygen in uranium–zirconium alloys is tightly linked to the extension of the O–U binary liquid miscibility gap in the ternary system at high zirconium content. Thus, in the two different sections presented by Politis [81] and revised by Skokan [85], a miscibility gap is presented in dotted line above 2673 K, but only extrapolated from the low temperature limit of solubility of oxygen measurements. Normally, the highest the solubility will be, the smallest the miscibility gap will be. The monotectic temperature separating the two-phase region L_1 + fcc_C1 and the miscibility gap $L_1 + L_2$ is located between 2573 and 2673 K. The Skokan's revision will decrease the miscibility gap range. A tentative Zr–UO_2 vertical section was proposed by Juenke and White [80], the miscibility gap above approximately 2623 K, is larger, because the zirconium content is lower, but the limit of solubility of UO_2 in Zr in the temperature range 2273–2673 K remains very imprecise. The solubilities of UO_2 in Zr, α-Zr(O) have been determined by Hayward and George [90, 91] over the temperature range 2273–2773 K. The UO_{2-x}–$ZrO_{0.54}$ vertical section has been graphically reported in the original paper [91]. In contrary to Skokan [85], these authors observed no microstructural evidence or step changes in solubility to indicate the presence of a two-liquid region in this section. They also measured the solubilities of UO_2 in U–Zr alloys at $T = 2373$ and 2473 K, allowing to measure the shape of the two-phase region $L1 + UO_{2-x}$ in this temperature range. Moreover, the oxygen solubility limit in the (U, Zr, O) liquid in the range 2020–2320 K for U/Zr = 1.5 determined by Maurisi et al. [14], 7 at.%, is lower than the one estimated by Politis [81] at 2273 K, 20 at.%, and was in favour of a low solubility of oxygen in the O–U binary liquid phase.

In our previous analysis [5], the low solubility values of O in U–Zr alloys determined by Politis [81] and Maurisi et al. [14] (2020–2320 K), seemed to be in contradiction with the higher ones of Hofman and Politis [84] (2273 K), Skokan [85] (2273–2473 K) and Hayward and George [90, 91] (2273–2773 K); moreover, the existence of a liquid miscibility gap in the pseudo-binary section UO_{2-x}–α(ZrO), presented by Politis [81] and extrapolated by Skokan [85], was put in question by the recent work of Hayward and George [91].

In the present analysis, all these results are not in contradiction, but determined at various zirconium contents, and thus might be conciliated by adopting a curvature of the phase limit $L_1 \Leftrightarrow L_1 + (U, Zr)O_{2-x}$ varying from a low solubility of oxygen on the O–U binary side towards a high solubility of oxygen on the O–Zr binary side. At a given zirconium content, the miscibility gap will disappear on the vertical section $ZrO_x + UO_2$, if x exceeds a certain limit. Moreover, the shape of the two-phase region $(U, Zr)O_{2-x} + L_1$ and the orientation of the tie lines in the temperature range 2273–2473 K is closely linked to the temperature and composition range of the triphasic domain $(U, Zr)O_{2-x} + L_1 + L_2$, which may occur between 2373 and 2673 K. We will see in the following how the new available experimental results validate this interpretation.

4.3.2. *Validation of the present analysis by new available experimental works*

Now, new experiments are available. In the hypostoichiometric field, a tie line of the liquid miscibility gap (Gueneau et al. [13]) in both O–U and O–U–Zr systems, and liquidus and solidus temperatures of six compositions in the UO_2–ZrO_2–Zr region representative of BWR and PWR configurations (Farmer et al. [92]).

On the one hand, the experimental study of Gueneau et al. [13] gives only one tie line in the O–U system, and thus, the selected errors affected to the phase limits may play a role on the extrapolation of the miscibility gap at high temperature and the critical temperature $L_1 \Leftrightarrow L_2$. In the ternary system, the global composition $x_O = 0.4$, $x_U = 0.4$, $x_{Zr} = 0.2$ varied due to vaporisation, but is located in the miscibility gap domain, not too far from the O–U side. In the analysis of the experimental results, the uncertainty affected both to the composition and temperature may play a role on the extrapolation of the miscibility gap at high zirconium content. In the present analysis, the experimental tie line is compatible with the existence of the $L_1 + L_2$ two-phase region over a wide range of temperature, between 2573 and 3273 K, and in the covered composition range.

On the other hand, the experimental points of Farmer et al. [92] are located on the two vertical sections O–$(U_{0.62}Zr_{0.38})$ for the PWR configuration and O–$(U_{0.41}Zr_{0.59})$ for the BWR configuration. Evidence of a liquid miscibility gap was not found for any one of the studied compositions.

These two experimental studies are quite compatible, and the two isopleth sections O–$(U_{0.62}Zr_{0.38})$ and O–$(U_{0.41}Zr_{0.59})$ should clearly show the presence of a liquid miscibility gap, with the following domains at high temperature, L_1 + fcc_C1, $L_1 + L_2$ + fcc_C1 and $L_1 + L_2$. The experimental points of Farmer et al. [92] are located at high UO_2 content, and thus in the two-phase region L_2 + fcc_C1. The experimental composition analysed by Gueneau et al. [13] is located at low UO_2 content, and thus in the $L_1 + L_2$ domain at high temperature (above 2573 K).

However, the less oxidised points are located very near the vertical section UO_2–$ZrO_{0.43}$. As for the previous results of Hayward and George [91] concerning the UO_{2-x}–$ZrO_{0.54}$ vertical section, no miscibility gap was found, in contradiction with the revised section proposed by Skokan [85]. Actually, this controversy is still difficult to resolve definitively, because it interests points located at high zirconium content for which no new measurement is available, and also in a domain in which the transition between a two-phase region L_1 + fcc_C1 and $L_1 + L_2$, or $L_1 + L_2$ and L, will be very sensible to temperature and composition variations.

5. Optimisation results

All the binary and quasi-binary Gibbs energy parameters have been previously evaluated in the critical assessment of the O–U, O–Zr, U–Zr and O_2U–O_2Zr systems, and are reported in Tables 1–3.

Ternary interaction parameters were generated by the thermodynamic modelling of the liquid, fcc_C1, hcp_A3 and bcc_A2 solution phases. Some of them were evaluated by hand from simple assumptions. The hcp_A3 ternary interaction parameter $L(O_1)_{0.5}(U_1, Zr_1)_1$ was estimated to reproduce a maximal solubility of uranium in the hcp_A3 solid solution equal to about 2 at.% at all temperatures. The bcc_A2 ternary interaction parameter $L(O_1)_3(U_1, Zr_1)_1$ was taken identical to the hcp_A3 previous one in the absence of ternary experimental information. The two last ternary parameters of the fcc_C1 solid solution, $L(U_1, Zr_1)_1(O_1)_2(O_1)_1$ and $L(U_1, Zr_1)_1(\square)_2(O_1)_1$, concern either the hyperstoichiometric field, interaction between O_3U_1(fcc_C1) and O_3Zr_1(fcc_C1), in which the only experimental information is the work of Punni and Mignanelli [67], or the hypostoichiometric field, interaction between O_1U_1(fcc_C1) and O_1Zr_1(fcc_C1), which are very metastable substances. Provisionally, they have been set to zero, but the first one could be estimated (from the experiments). The actual model generates a very rapid decrease of the deviation from stoichiometry x in UO_{2+x} with addition of zirconium, and a demixion between UO_{2+x} and $(U, Zr)O_{2+y}$, y being very small. Finally, only three ternary interaction parameters, $L(O_2U_1, Zr_1)_1$ and $L(O_2Zr_1, U_1)_1$ in the liquid phase, L, and $L(U_1, Zr_1)_1(\square)_2(\square)_1$ in the fcc_C1 solid solution have to be precisely evaluated to reproduce as well as possible the selected solubility of oxygen in liquid uranium–zirconium alloys and the shape of the two-phase region $(U, Zr)O_{2-x} + L_1$ [14, 81, 85, 90, 91] in the temperature range 2073–2773 K, the tie line of the miscibility gap [13] and the liquidus and solidus temperatures [67, 92]. In this work, the three ternary parameters of the liquid and fcc_C1 solid solution were evaluated by using the Parrot optimisation software [7] in close connection with an intelligent approach based on the method of trial and error. All the assessed ternary interaction parameters have been reported in Table 3.

The gas phase was treated as an ideal mixture of pure gaseous species, with the formula $(O_1, O_1U_1, O_1Zr_1, O_2, O_2U_1, O_2Zr_1, O_3, O_3U_1, U_1, Zr_1, Zr_2)_1$. The thermodynamic data of the gaseous species were directly taken from the THERMODATA substance database [9] and are reported in Table 4. The data of oxygen–uranium species have been recently reviewed by Cheynet and Chaud [10].

The O–U–Zr equilibrium phase diagram was calculated by using the calculation code GEMINI2 (Gibbs energy minimiser) available in the ThermoSuite software presented by Cheynet et al. [9]. Calculation results are graphically represented as isothermal sections in the temperature range 1273–3173 K on Figs. 5–17, and characteristical vertical sections (UO_2–Zr, UO_2–$ZrO_{0.43}$) on Figs. 18 and 19. The overall agreement with the surimposed experimental points was checked in order to evaluate the remaining uncertainties or insufficient knowledge.

6. Comparison between the calculated and experimental ternary phase diagram

The available experimental information was compared to the calculated ternary phase diagram both on isothermal sections (Figs. 5–17) and vertical sections (Figs. 18 and 19). In the following, we will distinguish three temperature ranges: a low temperature one, located between 1273 and 1973 K, an intermediate one, from 2073 to 2473 K, and a high temperature range, located between 2573 and 3173 K.

6.1. 1273–1973 K

The topology of the phase diagram is in qualitative agreement with the experimental works of Politis [81] and Yamanaka et al. [86] at 1273 K, and Saller et al. [79] at 1373 K. The diphasic and triphasic domains fcc_C1 + hcp_A3, fcc_C1 + hcp_A3 + bcc_A2 and hcp_A3 + bcc_A2 have been calculated, but a relative uncertainty still remains for the accurate composition of the phases in the triphasic domain. In particular, the compositions experimentally located in the fcc_C1 + hcp_A3 field by Saller et al. [79] would involve a solubility of uranium in the hcp_A3 solid solution higher than the one experimentally found at higher temperature.

No experimental data exists at 1473 and 1573 K.

The topology of the phase diagram at 1773 K is in qualitative agreement with the experimental results of Yamanaka et al. [87] at 1673 K and Politis [81] at 1773 K, showing two triphasic domains fcc_C1 + hcp_A3 + L and hcp_A3 + L + bcc_A2, the inversion with the topology fcc_C1 + hcp_A3 + bcc_A2 and fcc_C1 + bcc_A2 + L occurring at 1704 K.

In the field located in the triangle UO_2–ZrO_2–$Zr_{0.7}O_{0.3}$, a two-phase field fcc_C1 + fcc_C1 appears at 1773 K, due to the invariant reaction fcc_C1 $\Leftrightarrow$ O_2Zr_1(tetragonal) + hcp_A3 in the O–Zr binary system around 1773 K. Consequently, a triphasic domain fcc_C1 + fcc_C1 + hcp_A3 will be present between 1773 and 1873 K, in the hypostoichiometric domain. A miscibility gap fcc_C1 + fcc_C1 will be also present in the hyperstoichiometric domain at all temperatures. The presence of the miscibility gap in the solid solution is due to the stabilisation of the metastable miscibility gap in the O_2U–O_2Zr quasi-binary system in the hypostoichiometric field and to the unknown deviation from stoichiometry of UO_{2+x} when Zr is added in the hyperstoichiometric field.

At 1873 and 1973 K, the real experimental information is nearly non-existent: the section reported at 1873 K (Politis [81]) is hypothetical, and points were located in the

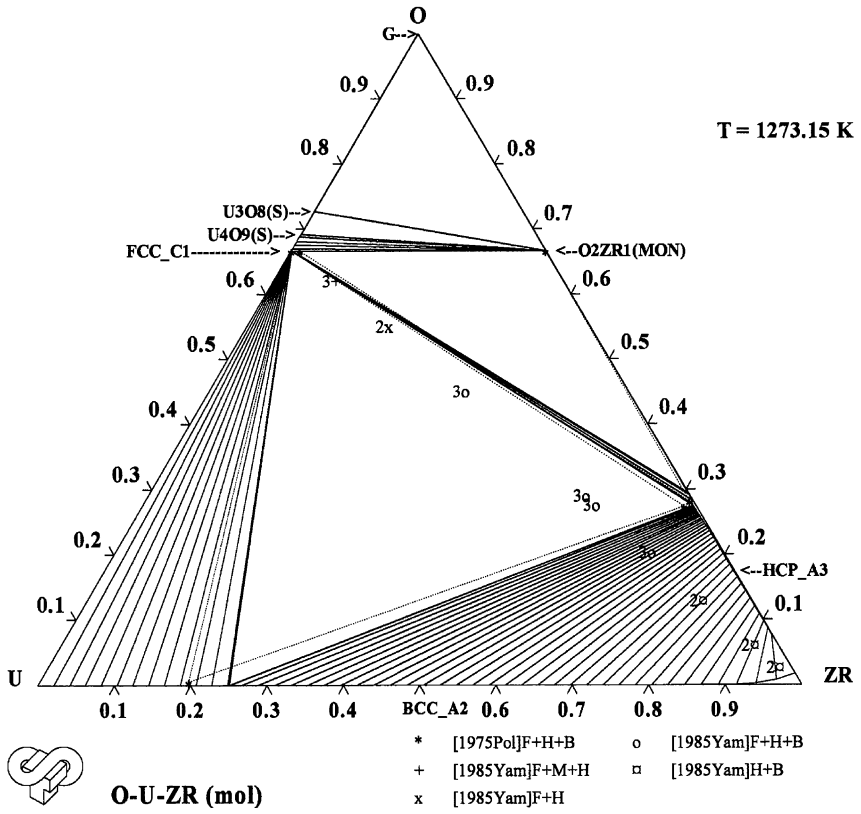

Fig. 5. Calculated O–U–Zr isothermal section at $T = 1273$ K compared to the selected experimental information.

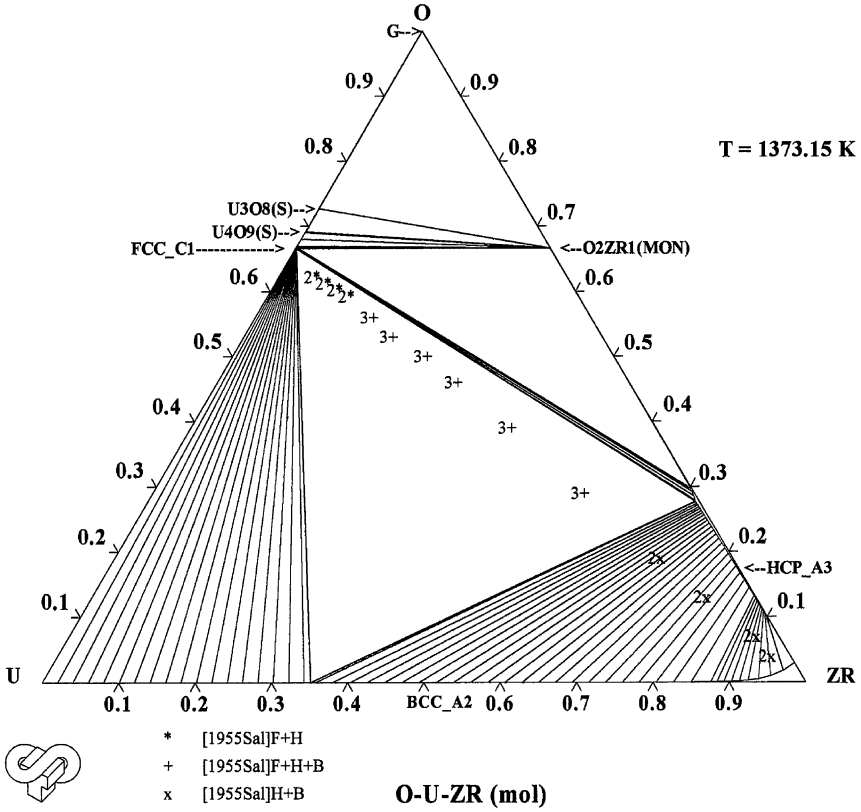

Fig. 6. Calculated O–U–Zr isothermal section at $T = 1373$ K compared to the selected experimental information.

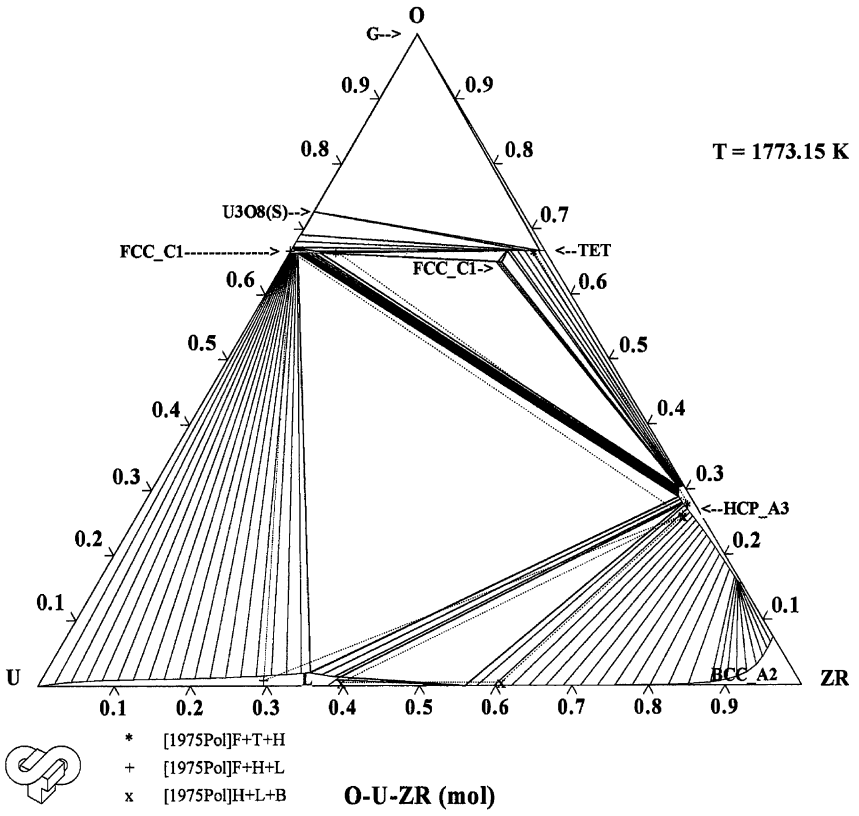

Fig. 7. Calculated O–U–Zr isothermal section at $T = 1773$ K compared to the selected experimental information.

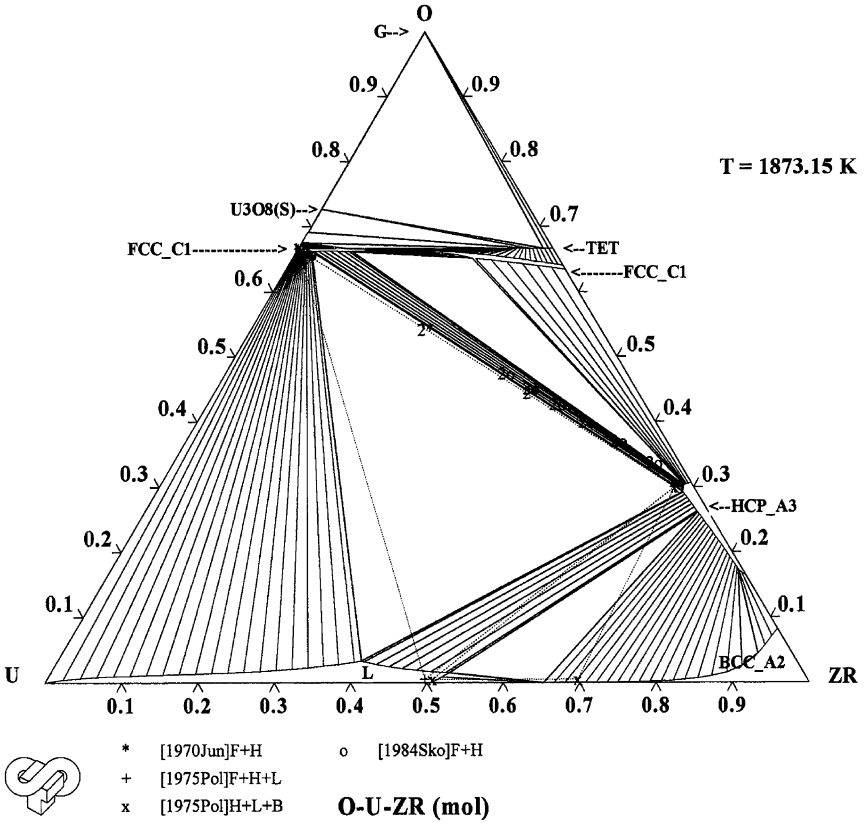

Fig. 8. Calculated O–U–Zr isothermal section at $T = 1873$ K compared to the selected experimental information.

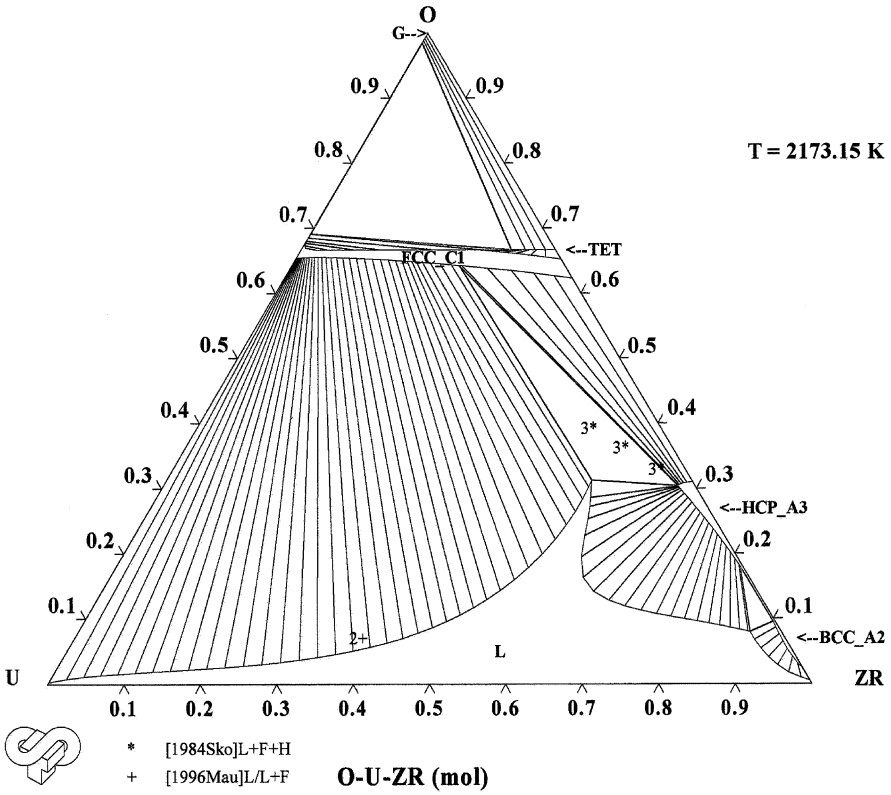

Fig. 9. Calculated O–U–Zr isothermal section at $T = 2173$ K compared to the selected experimental information.

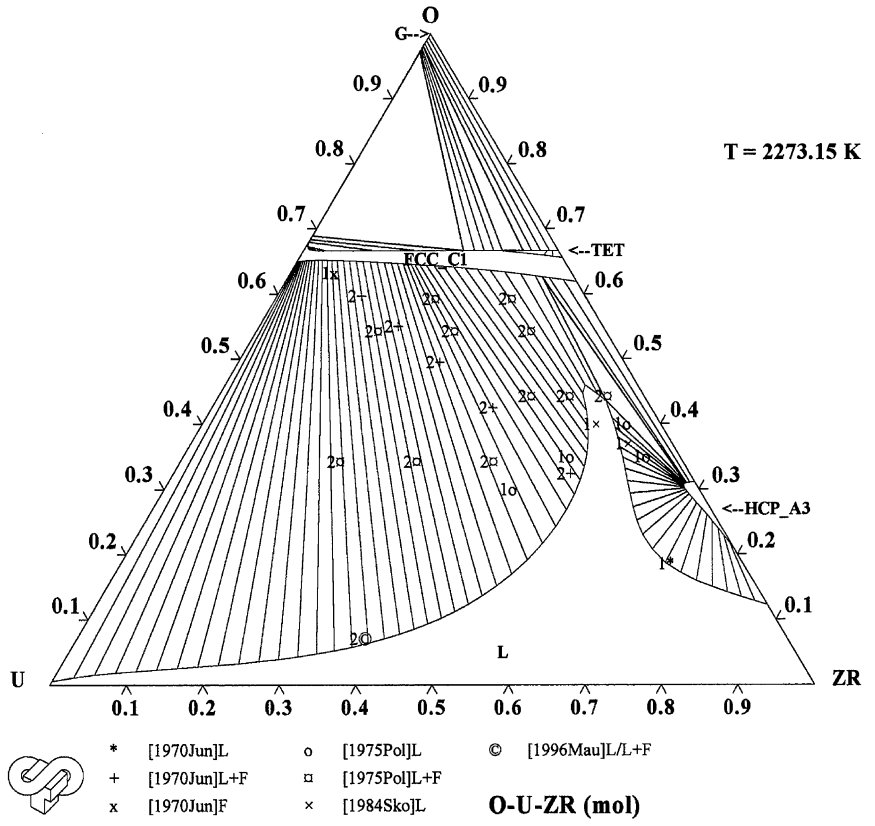

Fig. 10. Calculated O–U–Zr isothermal section at $T = 2273$ K compared to the selected experimental information.

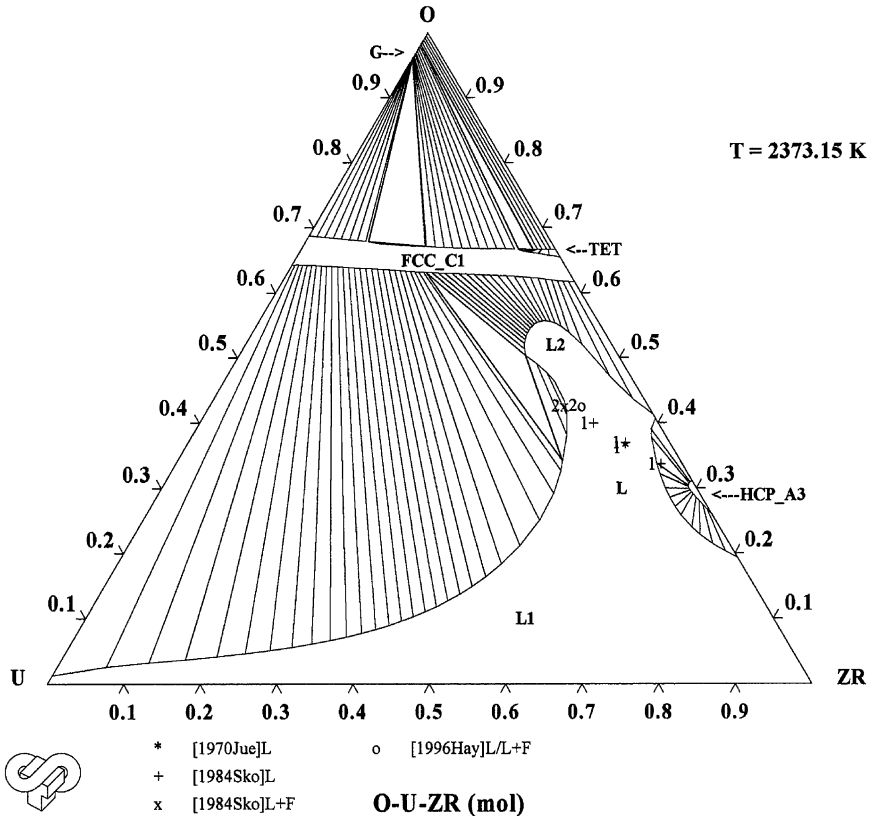

Fig. 11. Calculated O–U–Zr isothermal section at $T = 2373$ K compared to the selected experimental information.

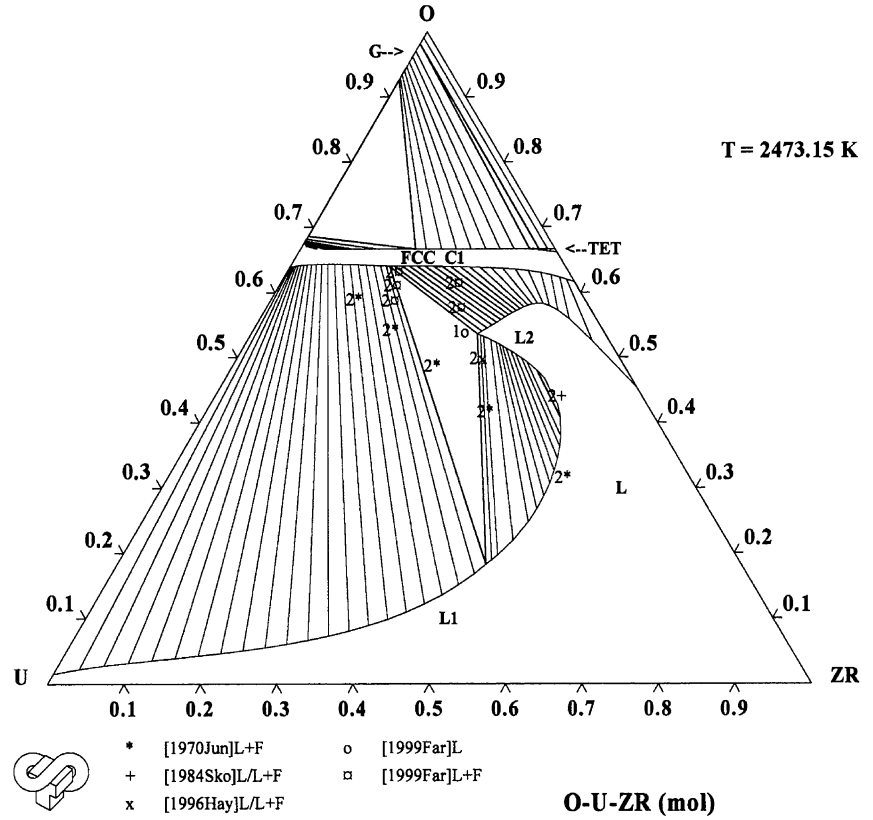

Fig. 12. Calculated O–U–Zr isothermal section at $T = 2473$ K compared to the selected experimental information.

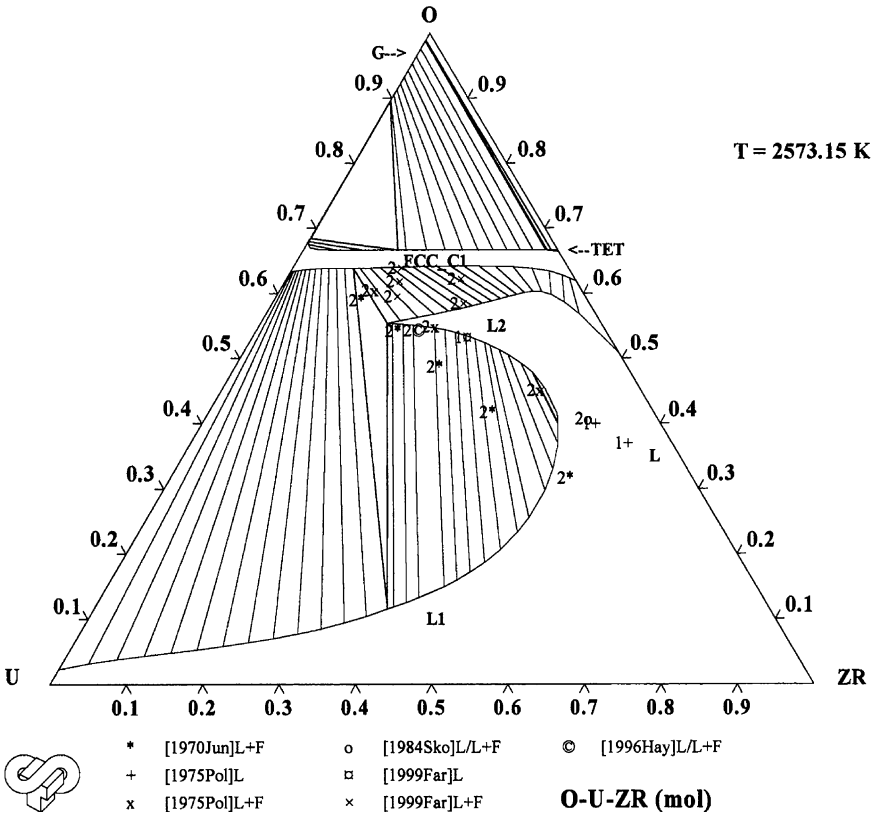

Fig. 13. Calculated O–U–Zr isothermal section at $T = 2573$ K compared to the selected experimental information.

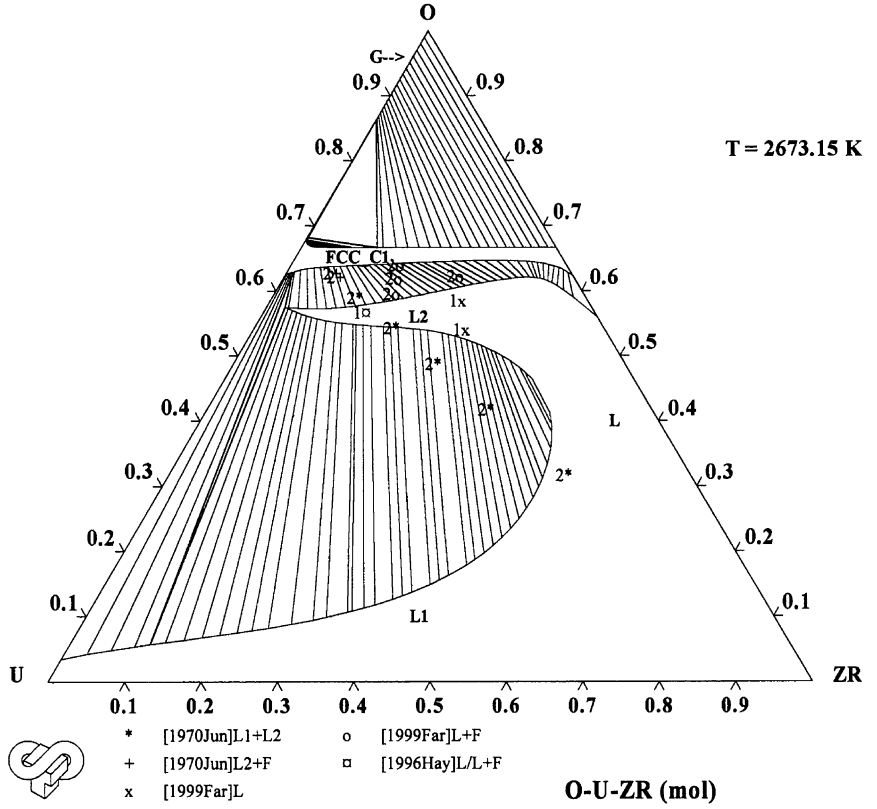

Fig. 14. Calculated O–U–Zr isothermal section at $T = 2673$ K compared to the selected experimental information.

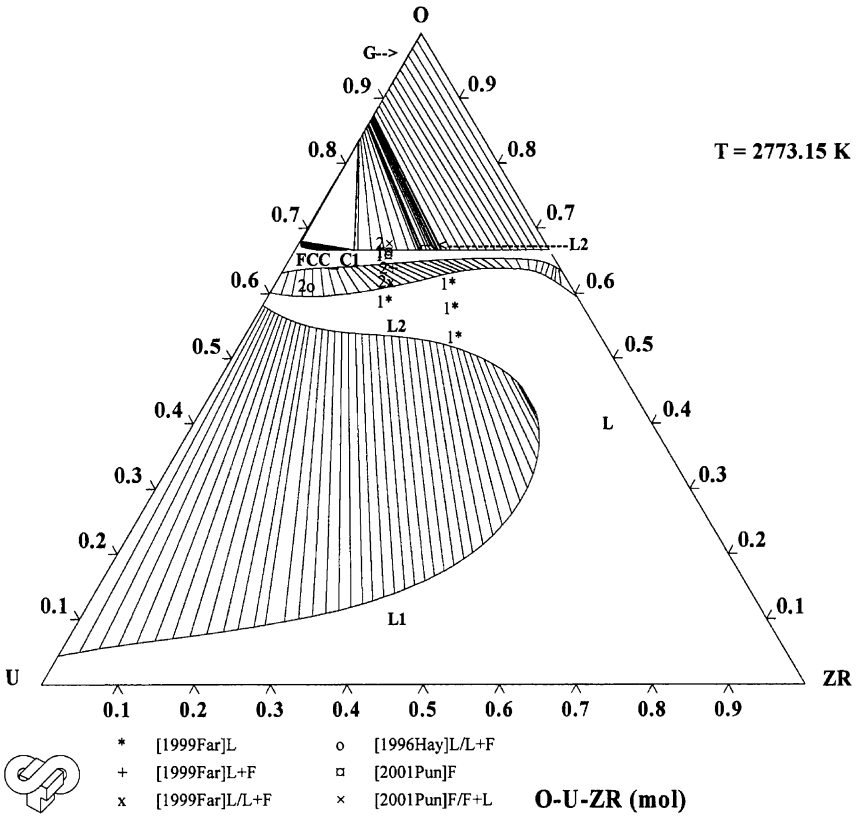

Fig. 15. Calculated O–U–Zr isothermal section at $T = 2773$ K compared to the selected experimental information.

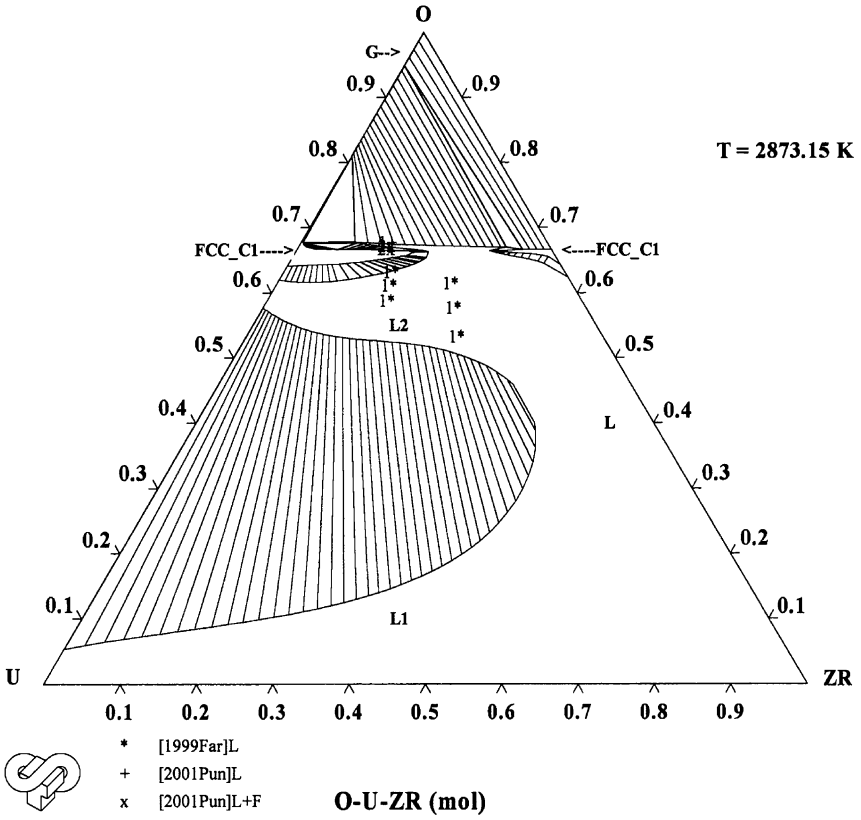

Fig. 16. Calculated O–U–Zr isothermal section at $T = 2873$ K compared to the selected experimental information.

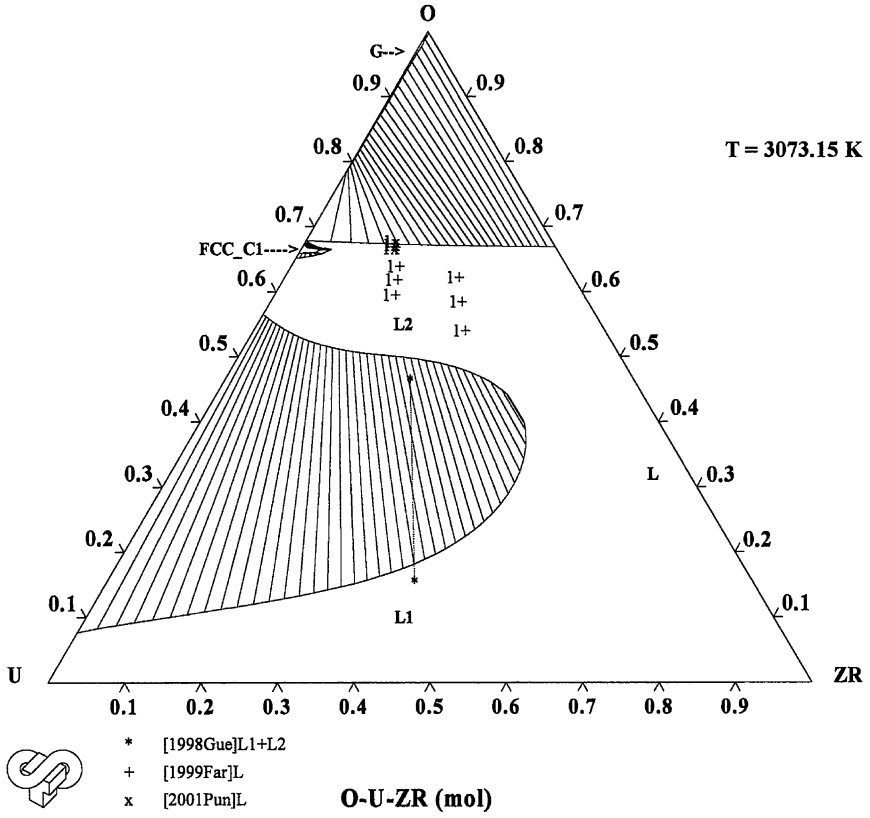

Fig. 17. Calculated O–U–Zr isothermal section at $T = 3073$ K compared to the selected experimental information.

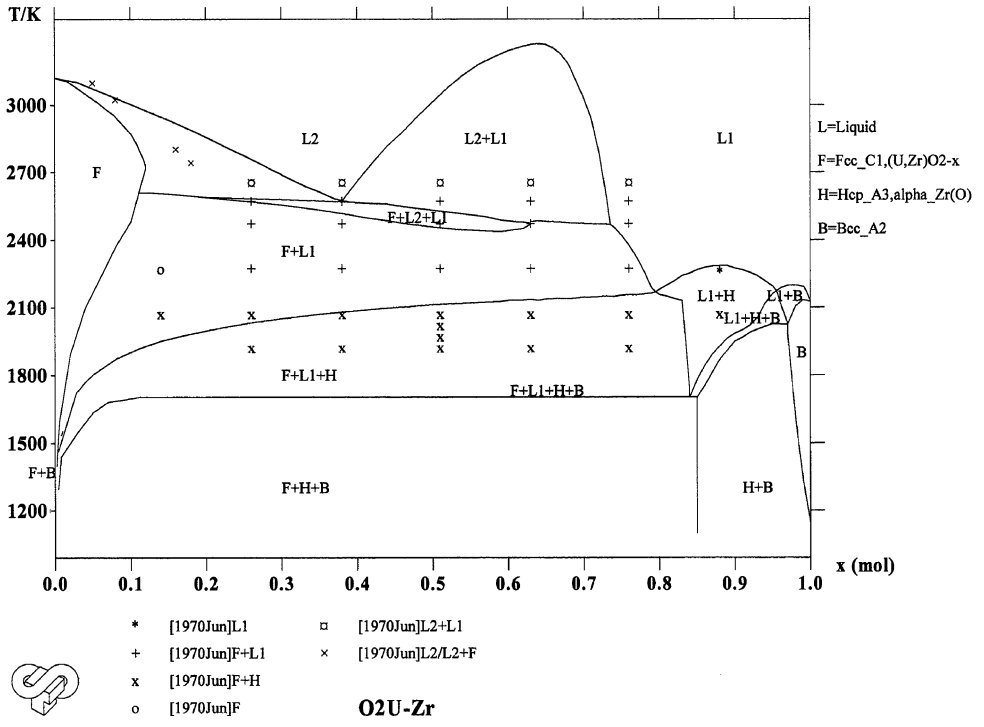

Fig. 18. Calculated O_2U–Zr vertical section compared to the available experimental points.

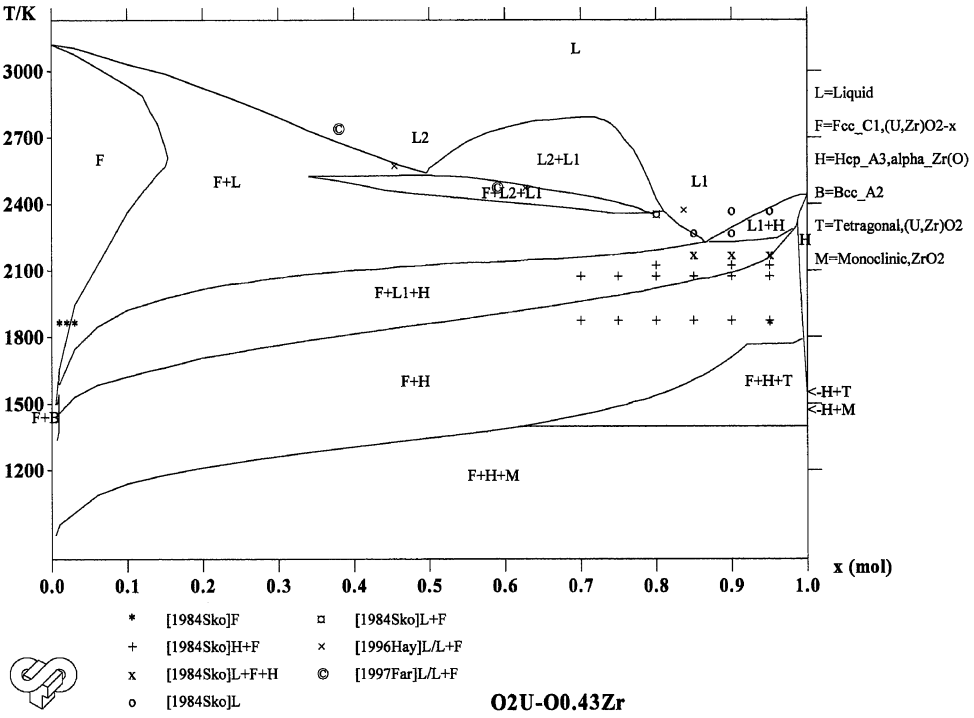

Fig. 19. Calculated O_2U–$O_{0.43}Zr$ vertical section compared to the available experimental points.

two-phase region fcc_C1 + hcp_A3 (Junke and White [80], Skokan [85]).

6.2. 2073–2473 K

In this intermediate temperature range, the experimental information is mainly located on the vertical sections UO_2–Zr (Junke and White [80]), UO_2–$ZrO_{0.43}$ (Politis [81], Skokan [85], or isothermal section (2273 K, [81]), giving points located either in the two-phase fields fcc_C1 + hcp_A3 and fcc_C1+L_1, or in the three-phase field fcc_C1+ hcp_A3 + L_1. At 2073 K, Junke and White [80] located points in the two-phase region fcc_C1 + hcp_A3. However, the limits of this two-phase region with the triphasic one fcc_C1 + hcp_A3 + L is very sensible with the oxygen content and temperature. The points on the section UO_2–Zr given by Junke and White [80] could be located in the triphasic domain. Due to uncertainties on the shape of the two-phase region fcc_C1 + L_1, measurements of the solubility of oxygen were made by Maurisi et al. [14] in the temperature range 2073–2273 K, but on the uranium rich side. On the zirconium rich side, the results of [81] and [85] are not too far. Recent experimental works of Hayward and George obtained from kinetics measurements [91] at 2373 and 2473 K indicate a very strong curvature of the liquidus on the zirconium rich side, in accordance with the Politis results at 2273 K. It can be noted that the shape of the liquidus on the zirconium rich side is in close connection with the shape of the liquidus in the O–Zr binary system, which is still insufficiently known. The recent liquidus measurements of Farmer et al. [92] are also in favour of this curvature. A miscibility gap appears in the liquid at high zirconium content between 2373 and 2473 K.

6.3. 2573–3173 K

In this temperature range, on a qualitative point of view, the topology of the phase diagram is characterised in the hypostoichiometric domain by the extension of the ternary liquid miscibility gap issued from the O–U liquid miscibility gap, leading to the two-phase regions L_1 + fcc_C1, L_2 + fcc_C1, and L_1 + L_2, and the triphasic domain L_1 + L_2 + fcc_C1. On a quantitative point of view, recent experimental results are available, concerning either a tie line in the liquid miscibility gap (Gueneau et al. [13]) and liquidus and solidus temperatures (Farmer et al. [92]) for compositions typical of PWR and BWR configurations. The experimental tie line (3223 ± 100 K) is in good agreement with the calculated ones in a wide range of temperatures, from 2973 to 3173 K, allowing an enlargement of the temperature uncertainty. The extrapolation of the miscibility gap at high zirconium content gives an orientation of the tie lines in the direction UO_2–Zr, and not in the inverse direction ZrO_2–U. A change in the orientation of the tie-lines would need a re-optimisation of the ternary parameters, but is not experimentally certain. The most recent experimental results on the liquidus and solidus of specific corium compositions corresponding either to PWR or BWR configurations in different states of oxidation [92] were compared numerically to the calculated ones in Table 5 (given in Appendix) and graphically reported on the isothermal sections (Fig. 13 to 17). The agreement for the solidus temperatures is not as

satisfactory, certainly because the phase transitions are not easily experimentally determinable, and due to the sensible shape of the L + fcc_C1 + hcp_A3. Thus, the solidus points will need further examinations. The experimental work of Farmer et al. [92] is in agreement with the experimental work of Hayward and George [91] and does not indicate an extension of the O–U binary liquid miscibility gap far beyond the ternary section UO_2–$ZrO_{0.43}$.

In the over-stoichiometric domain, the agreement with the experimental results of Punni and Mignanelli [67] is quite satisfactory for the liquidus and solidus temperatures. The presence of an hyperstoichiometric liquid in equilibrium with the gas phase at temperature above 2773 K and 1 atm is connected with the O–U optimisation.

6.4. Isopleth sections (UO_2–Zr, UO_2–$ZrO_{0.43}$)

A common feature of these sections is to present at high temperature the following diphasic and triphasic domains of interest for severe accidents: L, $L_1 + L_2$, L_2 + fcc_C1, L_1+fcc_C1, L_1+hcp_A3, L_1+hcp_A3+fcc_C1, hcp_A3+fcc_C1. The presence of a wide triphasic domain L_1 + hcp_A3 + fcc_C1 can explain the apparant incoherencies of the experimental vertical sections. The slope of the liquidus explains also the difficulty to extrapolate the liquid miscibility gap from solubility measurements.

7. Identified uncertainties or insufficient knowledge

Some uncertainties or domains insufficiently known have been identified in the present work, concerning both binary and ternary systems. We will indicate only the ones which are important for the nuclear accident field.

Concerning the O–U binary system, the shape of the miscibility gap in the hypostoichiometric field is based on only one tie line (Gueneau et al. [13]), and the oxygen solubility in liquid uranium deduced from this tie line and from measurements in the ternary system. In the hyperstoichiometric field, the temperature of the invariant reaction $L_2 \Leftrightarrow UO_{2+x}$ + G at 1 atm is unknown (Roth et al. [21]). These two points are particularly important and may play a role on the extension of the ternary liquid miscibility gap in reducing conditions and the degradation of the ceramic by liquefaction at temperatures decreasing versus pressure in oxidizing conditions.

Concerning the O–Zr system, the shape of the liquidus $L_1/ZrO_{2-x} + L_1$ is not precisely known.

Concerning the U–Zr binary and O_2U–O_2Zr quasi-binary systems, an important indetermination remains for the Gibbs energy level of solution phases, liquid, bcc_A2 and fcc_C1 at very high temperatures, i.e. between 2573 and 3273 K. In fact, activity measurements exist only below 1800 K for the first system, and up to 2500 K for the second one. In the two cases, the extrapolation of the Gibbs energy up to very high temperature must be realistic, and assessments leading to excess Gibbs energy more and more negative with increasing temperature must be carefully analysed (Leibowitz et al. [55], Ogawa and Iwai [54]).

Concerning the O–U–Zr ternary system, it seems now that the overall topology of the phase diagram is thermodynamically assessed over the whole temperature range 1273–3173 K.

At low temperatures, below 2000 K, the remaining uncertainties are only quantitative, such as the accurate compositions of the phases in the triphasic domains, or the solubility of uranium in the hcp_A3 solid solution.

At high temperature, above 2500 K, the more recent experimental results (Gueneau et al. [13], Farmer et al. [92], Punni and Mignanelli [67]) are satisfactorily reproduced, and all the remaining uncertainties are located in the UO_2–ZrO_2–Zr triangle, such as the orientation of the tie lines or liquidus temperatures. However, the present modelling does not predict the extension of the liquid miscibility gap far beyond the line UO_2–$ZrO_{0.43}$, while it is present on the vertical sections for O–$U_{0.62}Zr_{0.38}$, O–$U_{0.41}Zr_{0.59}$ and UO_2–Zr. Any proposed measurement should be carefully analysed, due to the difficulty of experiments and associated errors.

Finally, additional experiments in the medium temperature range, 2000–2500 K, appear to be the most useful.

8. Conclusion

In this work, a new thermodynamic modelling of the ternary O–U–Zr system was performed on the basis of a preliminary improvement of the thermodynamic modelling of all binary and quasi-binary sub-systems, i.e. O–U, O–Zr, O_2U–O_2Zr and U–Zr, followed by an evaluation of ternary interaction parameters in the main solution phases, i.e. liquid (L), ceramic $(U, Zr)O_{2+x}$ (fcc_C1) and Zr-O–U (hcp_A3, bcc_A2) solid solutions, from the critical analysis of all the selected available experimental information. A very sensible improvement with regards to our previous work has been obtained.

On a qualitative point of view, the overall topology of the O–U–Zr ternary phase diagram has been assessed over the whole temperature range, between 1273 and 3173 K.

On a quantitative point of view, the solubility of oxygen in uranium–zirconium liquid alloys, the liquid miscibility gap and the liquidus and solidus temperatures of the selected authors have been conciliated and the obtained agreement represented by means of isothermal and isopleth sections.

The remaining uncertainties or insufficient knowledge concern mainly in the hypostoichiometric field, the accurate shape of the domains in the intermediate temperature range 2000–2500 K. Further experiments in this field could improve the accuracy of the thermodynamic modelling and its extrapolation power at higher temperature, such as the orientation of the tie lines in the UO_2–ZrO_2–Zr triangle, in which direct experiments are very difficult at temperatures above 2500 K. In the hyperstoichiometric field, the isobars on the liquidus have to be determined.

Table 5
Comparison between the calculated and experimental liquidus

Representating reactor configuration	x(O)	x(U) Atomic fraction	x(Zr)	T^{L}(exp) (K)	T^{L}(calc) (K)	ΔT	T^{S}(exp) (K)	T^{S}(calc) (K)	ΔT
[92]									
N°5 (PWR, 30% ox.)	0.595 35	0.251 65	0.153 00	2738-29/+21	2714	−24			
N°4 (PWR, 50% ox.)	0.618 44	0.236 96	0.144 60	2773-29/+21	2812	+49			
N°6 (PWR, 70% ox.)	0.639 45	0.224 10	0.136 45	2793-29/+21	2898	+105			
N°8 (BWR, 30% ox.)	0.539 74	0.187 97	0.272 29	2472-26/+18	2498	+26			
N°7 (BWR, 50% ox.)	0.584 38	0.169 77	0.245 85	2603-27/+19	2598	−5			
N°9 (BWR, 70% ox.)	0.622 00	0.154 62	0.223 38	2748-29/+21	2740	−8			
ΔT(mean)						37			
[67]									
$U_{0.65}Zr_{0.35}O_{2.000}$	0.666 67	0.216 67	0.116 67	2951	2936	−15	2863	2877	+14
$U_{0.65}Zr_{0.35}O_{2.052}$	0.672 35	0.212 97	0.114 68	2911	2858	−53	2823	2790	−33
$U_{0.65}Zr_{0.35}O_{2.098}$	0.677 211	0.209 81	0.112 97	2834	2804	−30	2755	2789	+34
ΔT(mean)						33			
ΔT(mean, all)						35			27

The sublattice model used for all the solid solutions, fcc_C1, hcp_A3 and bcc_A2, is well adapted for the purpose.

The non-ideal associate model used for the liquid phase allowed us to obtain a satisfactory self-consistency of all the selected experimental information.

Further improvements will have to be done in the theoretical extrapolation of the excess Gibbs energy of the uranium–zirconium liquid phase at very high temperatures (3000 K) and in the experimental determination of tie lines in the two-phase region L_1 + fcc_C1 at intermediate temperatures (2000–2500 K).

The optimisation of ternary parameters is highly dependant of the quality of the Gibbs energy level of the sub-systems and of the selected ternary experimental information. These two points have to be clarified to increase the capability of the model for extrapolating in experimentally unexplored domains.

The definition of the standards to be used is a crucial point for the building of a solution thermodynamic database for nuclear applications, in order to increase the basic knowledge and to feed more global thermohydraulic codes dedicated to severe accidents.

Acknowledgements

This work was executed under the multi-partners project “ENTHALPY” (European nuclear thermodynamic database validated and applicable in severe accident codes), co-financed by the European Commission under the 5th FrameWork Programme of the Euratom for Research and Training in the Field of Nuclear Energies (1998–2002). The authors wish to thank all the partners: AEA-T, AEKI, CEA, EDF, FRAMATOME-ANP, IRSN, SCK, SKODA, THERMODATA, UCL, ULB, for valuable technical discussions, and in particular IRSN for its financial support.

Appendix

Table 5.

References

[1] P.Y. Chevalier, E. Fischer, B. Cheynet, A. Rivet, G. Cenerino, J. Chim. Phys. 94 (1997) 849.
[2] B. Cheynet, P. Chaud, P.Y. Chevalier, E. Fischer, P. Mason, M. Mignanelli, J. Chim. Phys. (2003) (in press).
[3] B. Adroguer, G. Azarian, M. Barrachin, M. Bellon, D. Bottomley, P.Y. Chevalier, B. Cheynet, G. Cognet, M. Coquerelle, M. Fischer, K. Forcey, P. Hofman, S. Hellmann, S. Marget, R. Nannicini, J.M. Seiler, P. Pacenti, M. Steinbrück, F. Toci, Corium interactions and thermochemistry (CIT Project), In-vessel core degradation and coolability (INV cluster), In and ex-vessel corium properties and thermochemistry, Fisa-1999, EU Research in Reactor Safety, EC, Luxembourg, 29 November–1 December, 1999.
[4] A. De Bremaecker, M. Barrachin, L. Belovsky, P.Y. Chevalier, B. Cheynet, F. Defoort, P.H. Duvigneaud, K. Froment, F. Funke, S. Hellmann, Z. Hozer, F. Jacq, C. Journeau, S. Marguet, P. Mason, K. Mwamba, M. Mignanelli, P. Piluso, C. Ronneau, L. Sannen, M. Verwerft, V. Vrilkova, European nuclear thermodynamic database for in & ex-vessel applications (ENTHALPY), Fisa-2003, EU Research on Severe Accidents, EC, Luxembourg, 10–13 November, 2003.
[5] P.Y. Chevalier, E. Fischer, J. Nucl. Mater. 257 (1998) 213.
[6] H.L. Lukas, E.Th. Henig, B. Zimmermann, Calphad 1 (3) (1977) 225.
[7] J.-O. Andersson, T. Helander, L. Höglund, P. Shi, B. Sundman, Calphad 26 (2002) 273–312.
[8] A.T. Dinsdale, Calphad 15 (4) (1991) 317.
[9] B. Cheynet, P.Y. Chevalier, E. Fischer, Calphad 26 (2) (2002) 167–174.
[10] B. Cheynet, P. Chaud, ENTHALPY Project, SAM-ENTHA(03)-D022, March, 2003.
[11] P.Y. Chevalier, E. Fischer, B. Cheynet, Calphad XXX, York, England, 31st May, 2001.
[12] P.Y. Chevalier, E. Fischer, B. Cheynet, J. Nucl. Mater. 303 (2002) 1.
[13] C. Gueneau, V. Dauvois, P. Perodeaud, C. Gonella, O. Dugne, J. Nucl. Mater. 254 (1998) 158.
[14] A. Maurisi, C. Gueneau, P. Perodeaud, B. Schneider, O. Dugne, F. Valin, G. Bordier, Proc. Int. Conf. EUROMAT, October, 1996.
[15] M. Baichi, INPG Thesis, September, 2001.
[16] M. Baichi, C. Chatillon, C. Gueneau, J. Le Ny, J. Nucl. Mater. 303 (2002) 196.

[17] D. Labroche, INPG Thesis, September, 2000.
[18] D. Labroche, O. Dugne, C. Chatillon, J. Nucl. Mater. 312 (2003) 21, 50.
[19] C. Gueneau, M. Baichi, D. Labroche, C. Chatillon, B. Sundman, J. Nucl. Mater. 304 (2002) 161.
[20] P.K. Mason, M.A. Mignanelli, (ENTHALPY project), SAM-ENTHA(02)-D017, August 2002-AEAT/R/NS/0582.
[21] R.S. Roth, T. Negas, L.P. Cook, Phase Diagrams for Ceramists, vol. IV, Am. Ceram. Soc., 1981 (Figures 5000–5590).
Yu.V. Levinskii, At. Energ. 37 (4) (1974) 339; Sov. At. Energy (Engl. Transl.) 37 (4) (1974) 1075; Figures 5028 reported by R.S. Roth, T. Negas and L.P. Cook, Phase Diagrams for Ceramists, vol. IV, Am. Ceram. Soc., 1981 (Figures 5000–5590).
[22] Y. Saito, J. Nucl. Mater. 51 (1974) 112.
[23] P.L. Blum, P. Guinet, H. Vaugoyeau, C. R. Acad. Sci. 257 (22) (1963) 3401.
[24] J.L. Bates, U.S. At. Energy Comm., HW-81603 (1964) 2.15.
[25] A.E. Martin, R.K. Edwards, J. Phys. Chem. 69 (5) (1965) 1788;
R.K. Edwards, A.E. Martin, Thermodynamics of Nuclear Materials, vol. II, IAEA, Vienna, 1966, p. 423.
[26] J.L. Bates, J. Am. Ceram. Soc. 49 (7) (1966) 395.
[27] P. Guinet, H. Vaugoyeau, P.L. Blum, C. R. Acad. Sci., 263, Série C (4 juillet 1966), 17;
Rapport CEA-R3060, CENG, Section de Métallurgie Novembre, 1966.
[28] M.J. Bannister, J. Nucl. Mater. 24 (1967) 340.
[29] A. Kotlar, P. Gerdanian, M. Dodé, J. Chem. Phys. 65 (1968) 687.
[30] R.J. Ackermann, E.G. Rauh, M.S. Chandrasekharaiah, J. Phys. Chem. 73 (4) (1969) 762.
[31] R.E. Latta, R.E. Fryxell, J. Nucl. Mater. 35 (1970) 195.
[32] M. Tetenbaum, P.D. Hunt, J. Nucl. Mater. 34 (1970) 86.
[33] T. Matsui, K. Naito, J. Nucl. Mater. 56 (1975) 327.
[34] S.P. Garg, R.J. Ackermann, J. Nucl. Mater. 88 (1980) 309.
[35] R.F. Domagala, D.J. McPherson, J. Metals, Trans. AIME (1954) 238.
[36] B. Holmberg, A. Magneli, Acta Chem. Scand. 12 (6) (1958) 1341.
[37] E. Gebhardt, H.D. Seghezzi, W. Dürrschnabel, J. Nucl. Mater. 4 (3) (1961) 255.
[38] B. Holmberg, T. Dagerhamn, Acta Chem. Scand. 15 (4) (1961) 919.
[39] R. Ruh, H.J. Garrett, J. Am. Ceram. Soc. 50 (5) (1957) 257.
[40] A.N. Kornilov, I.M. Ushakova, S.M. Skuratov, G.P. Shveikin, Dok. Akad. Nauk SSSR 186 (4) (1969) 831.
[41] G. Boureau, P. Gerdanian, High Temp.-High Pressures 2 (1970) 681.
[42] R.J. Ackermann, S.P. Garg, E.G. Rauh, J. Am. Ceram. Soc. 60 (7–8) (1977) 341.
[43] R.J. Ackermann, S.P. Garg, E.G. Rauh, J. Am. Ceram. Soc. 61 (5–6) (1978) 275.
[44] R.J. Ackermann, S.P. Garg, E.G. Rauh, High Temp. Sci. 11 (1979) 199.
[45] E.G. Rauh, S.P. Garg, High Temp. Sci. 14 (1981) 121–134.
[46] G. Boureau, P. Gerdanian, J. Phys. Chem. Solids 45 (2) (1984) 141.
[47] J.P. Abriata, J. Garcès, R. Versaci, Bull. Alloy Phase Diagrams 7 (1986) 2.
[48] T. Tanabe, M. Tanaka, S. Imoto, Surf. Sci. 187 (1987) 499.
[49] P. Liang, H.J. Seifert, H.L. Lukas, S.G. Fries, N. Dupin, I. Ansara, F. Aldinger, Z. Metallkd. 92 (7) (2001) 747–756.
[50] R. Arroyave, L. Kaufman, T.W. Eager, Calphad 26 (1) (2002) 118.
[51] M. Kanno, M. Yamawaki, T. Koyama, N. Morioka, J. Nucl. Mater. 154 (1988) 154.
[52] A. Maeda, Y. Suzuki, T. Ohmichi, J. Alloys Compounds 179 (1992) L25.
[53] L. Leibowitz, R.A. Blomquist, A.D. Pelton, J. Nucl. Mater. 167 (1989) 76.
[54] T. Ogawa, T. Iwai, J. Less-Common Met. 170 (1991) 101.
[55] L. Leibowitz, E. Veleckis, R.A. Blomquist, A.D. Pelton, J. Nucl. Mater. 154 (1988) 145.
[56] D. Summers-Smith, J. Inst. Met. 83 (1954–1955) 277.
[57] J. Philibert, Y. Adda, C. R. Acad. Sci. (1957) 2507.
[58] J.F. Duffey, C.A. Bruch, Trans. Met. Soc. AIME (1958) 17.
[59] B.W. Howlett, A.G. Knapton, 2nd UN Int. Conf. on Peaceful Use of Atomic Energy, Geneva, vol. 6, 1958, p. 104.
[60] S.T. Zegler, Argonne National Laboratory Report, USAEC Rep.ANL-6055, 1962;
H.A. Saller, F.A. Rough, J.M. Fackelmann, A.A. Bauer, J.R. Doig, BMI-1023 (1955).
[61] T. Ohmichi, private communication: reported by Ogawa and Iwai [54].
[62] M. Akabori, A. Itoh, T. Ogawa, F. Kobayashi, Y. Suzuki, J. Nucl. Mater. 188 (1992) 249.
[63] O. Relave, P.Y. Chevalier, B. Cheynet, G. Cenerino, in: F.H. Hayes (Ed.), User Aspects of Phase Diagrams, Proceedings of the International Conference, The Joint Research Centre, Petten, The Netherlands, 25–27 June, 1990 (Organised jointly by the Institute of Metals and the Commission of the European Communities, Joint Research Centre, Institute for Advanced Materials, Petten), The Institute of Metals, 1991, pp. 55–63.
[64] P.Y. Chevalier, J. Nucl. Mater. 186 (1992) 212–225.
[65] R.G.J. Ball, M.A. Mignagnelli, T.I. Barry, J.A. Gisby, J. Nucl. Mater. 201 (1993) 238–249.
[66] M. Yashima, T. Koura, Y. Du, M. Yoshimura, J. Am. Ceram. Soc. 79 (2) (1996) 521–524.
[67] J.S. Punni, M.A. Mignanelli, ENTHALPY project, SAM-ENTHA(01) - D004, August, 2001, AEAT / R / NS / 0428.
[68] M. Baichi, C. Chatillon, C. Gueneau, S. Chatain, J. Nucl. Mater. 294 (2001) 84.
[69] W.A. Lambertson, M.H. Mueller, J. Am. Ceram. Soc. 36 (11) (1953) 367.
[70] N.M. Voronov, E.A. Voitekhova, A.S. Danilin, Proc. 2nd Genova Conf., vol. 6, 1958, p. 221.
[71] G.M. Wolten, J. Am. Chem. Soc. 80 (1958) 4772.
[72] P.E. Evans, J. Am. Ceram. Soc. 43 (9) (1960) 443.
[73] I. Cohen, B.E. Schaner, J. Nucl. Mat. 9 (1) (1963) 18.
[74] L.G. Wisnyi, S.W. Pijanowski, Knolls Atomic Power Laboratory (USA) Report, KAPL-1702, 1957.
[75] K.A. Romberger, C.F. Baes, H.H. Stone, J. Inorg. Nucl. Chem. 29 (1967) 1619.
[76] J.O.A. Pashoal, H. Kleykamp, F. Thümmler, J. Nucl. Mater. 151 (1987) 10.
[77] C.A. Alexander, J.S. Ogden, R.Y. Lee, High Temp. Mat. Sci. 33 (1995) 3.
[78] V. Stolyarova, A. Shilov, M. Shultz, J. Nucl. Mater. 247 (1997) 41.
[79] H.A. Saller, F.A. Rough, J.M. Fackelmann, A.A. Bauer, J.R. Doig, BMI-1023, 1955.
[80] E.F. Junke, J.F. White, GEMP-731, 1970.
[81] C. Politis, Gesellschaft für Kernforschung M.B.H., Karlsruhe, KFK 2167 Oktober, 1975, 1–53.
[82] D.L. Hagrman, G.A. Reymann, R.E. Mason, NUREG/CR-0479, TREE-1280, Rev. 2, R3 and R4, Inc. Idaho Falls, Idaho 83415, August, 1981.
[83] P. Hofman, H. Holleck, C. Politis, A. Skokan, Gesellschaft für Kernforschung M.B.H., Karlsruhe, KFK 2242, February, 1976, 1–3.
[84] P. Hofman, C. Politis, J. Nucl. Mater. 87 (2–3) (1979) 375.
[85] A. Skokan, Proc. 5th Int. Meeting on Thermonuclear reactor safety, Karlsruhe, September 9–13, 1984.
[86] S. Yamanaka, M. Katsura, M. Miyake, S. Imoto, S. Kawasaki, J. Nucl. Mater. 130 (1985) 524.
[87] S. Yamanaka, M. Katsura, S. Imoto, M. Miyake, Inorg. Chim. Acta 140 (1987) 127.
[88] M. Miyake, M. Katsura, S. Yamanaka, J. Nucl. Mater. 154 (1988) 123.
[89] P. Hofman, S.J.L. Hagen, G. Schanz, A. Skokan, Kernforschungszentrum Karlsruhe, KFK 4485, January, 1989. Nuclear technology 87 (1989) 146.
[90] P. Hayward, I.M. George, J. Nucl. Mater. 208 (1994) 35.
[91] P. Hayward, I.M. George, J. Nucl. Mater. 232 (1996) 1.
[92] M.T. Farmer, B.W. Spencer, R.W. Aeschlimann, in: OECD Workshop on Ex-Vessel Debris Coolability, Karlsruhe, Germany 15–19 November, 1999.